Cell Reports

Article

Precise Temporal Regulation of Post-transcriptional Repressors Is Required for an Orderly *Drosophila* Maternal-to-Zygotic Transition

Graphical Abstract

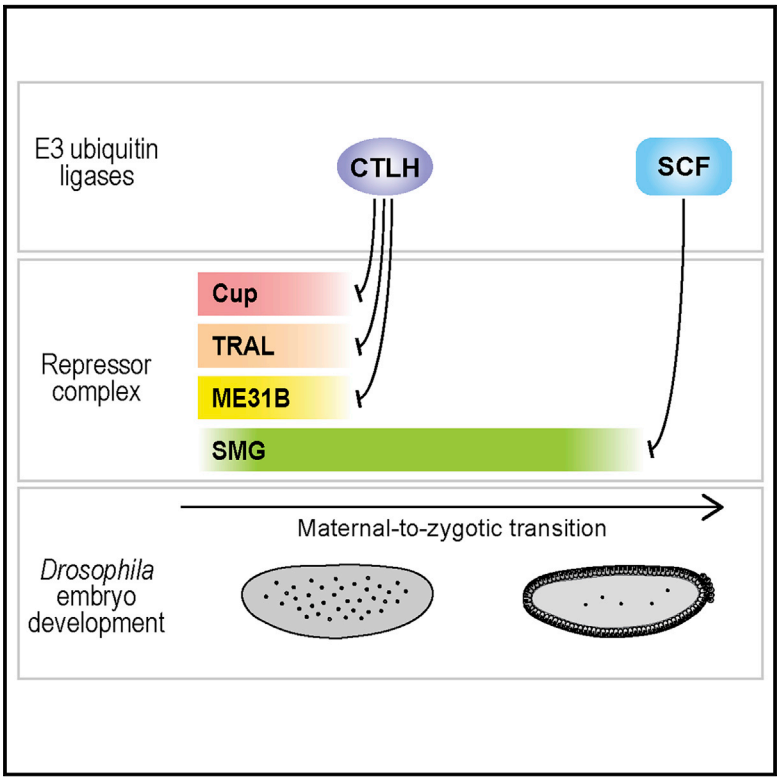

Authors

Wen Xi Cao, Sarah Kabelitz, Meera Gupta, ..., Martin Wühr, Elmar Wahle, Howard D. Lipshitz

Correspondence

elmar.wahle@biochemtech.uni-halle.de (E.W.), howard.lipshitz@utoronto.ca (H.D.L.)

In Brief

Cao et al. show that 2% of the proteome is degraded in early *Drosophila* embryos, including a repressive ribonucleoprotein complex. Two E3 ubiquitin ligases separately act on distinct components of this complex to phase their clearance. Failure to degrade a key component, the Smaug RNA-binding protein, disrupts an orderly maternal-to-zygotic transition.

Highlights

- Early *Drosophila* embryos degrade 2% of their maternally encoded proteome
- The Cup-TRAL-ME31B-Smaug post-transcriptional repressive complex is cleared
- Distinct E3 ubiquitin ligases target Cup-TRAL-ME31B (CTLH E3) versus Smaug (SCF E3)
- Failure to degrade Smaug abrogates an orderly maternal-to-zygotic transition

Cao et al., 2020, Cell Reports *31*, 107783
June 23, 2020 © 2020 The Author(s).
https://doi.org/10.1016/j.celrep.2020.107783

CellPress

Cell Reports

CellPress
OPEN ACCESS

Article

Precise Temporal Regulation of Post-transcriptional Repressors Is Required for an Orderly *Drosophila* Maternal-to-Zygotic Transition

Wen Xi Cao,[1] Sarah Kabelitz,[2] Meera Gupta,[3] Eyan Yeung,[3] Sichun Lin,[4] Christiane Rammelt,[2] Christian Ihling,[5] Filip Pekovic,[2] Timothy C.H. Low,[1] Najeeb U. Siddiqui,[1] Matthew H.K. Cheng,[6] Stephane Angers,[4,6] Craig A. Smibert,[1,6] Martin Wühr,[3] Elmar Wahle,[2,*] and Howard D. Lipshitz[1,7,*]

[1]Department of Molecular Genetics, University of Toronto, 661 University Avenue, Toronto, ON M5G 1M1, Canada
[2]Institute of Biochemistry and Biotechnology and Charles Tanford Protein Center, Martin Luther University Halle-Wittenberg, Kurt-Mothes-Str. 3, 06099 Halle, Germany
[3]Department of Molecular Biology and the Lewis-Sigler Institute, Princeton University, Washington Road, Princeton, NJ 08544, USA
[4]Department of Pharmaceutical Sciences, University of Toronto, 144 College Street, Toronto, ON M5S 3M2, Canada
[5]Institute of Pharmacy and Charles Tanford Protein Center, Martin Luther University Halle-Wittenberg, Kurt-Mothes-Str. 3, 06099 Halle, Germany
[6]Department of Biochemistry, University of Toronto, 661 University Avenue, Toronto, ON M5G 1M1, Canada
[7]Lead Contact
*Correspondence: elmar.wahle@biochemtech.uni-halle.de (E.W.), howard.lipshitz@utoronto.ca (H.D.L.)
https://doi.org/10.1016/j.celrep.2020.107783

SUMMARY

In animal embryos, the maternal-to-zygotic transition (MZT) hands developmental control from maternal to zygotic gene products. We show that the maternal proteome represents more than half of the protein-coding capacity of *Drosophila melanogaster*'s genome, and that 2% of this proteome is rapidly degraded during the MZT. Cleared proteins include the post-transcriptional repressors Cup, Trailer hitch (TRAL), Maternal expression at 31B (ME31B), and Smaug (SMG). Although the ubiquitin-proteasome system is necessary for clearance of these repressors, distinct E3 ligase complexes target them: the C-terminal to Lis1 Homology (CTLH) complex targets Cup, TRAL, and ME31B for degradation early in the MZT and the Skp/Cullin/F-box-containing (SCF) complex targets SMG at the end of the MZT. Deleting the C-terminal 233 amino acids of SMG abrogates F-box protein interaction and confers immunity to degradation. Persistent SMG downregulates zygotic re-expression of mRNAs whose maternal contribution is degraded by SMG. Thus, clearance of SMG permits an orderly MZT.

INTRODUCTION

Embryonic development in all animals begins with the maternal-to-zygotic transition (MZT) (reviewed in Tadros and Lipshitz, 2009; Vastenhouw et al., 2019). The MZT can be divided into two phases: initially, maternally supplied RNAs and proteins direct embryonic development; subsequently, activation of transcription from the zygotic genome, a process termed "zygotic genome activation" (ZGA), transfers developmental control from the mother's genome to that of the embryo. During the first phase, post-transcriptional regulation of maternal transcripts and post-translational regulation of maternal proteins predominate. The former is coordinated by RNA-binding proteins (RBPs), which regulate the translation, stability, and localization of the maternal transcripts. A large proportion of maternal mRNA species is degraded in a highly coordinated manner during the MZT (Aanes et al., 2014; De Renzis et al., 2007; Laver et al., 2015; Stoeckius et al., 2014; Svoboda et al., 2015; Tadros et al., 2007; Thomsen et al., 2010). Transcriptome-wide changes in the translational status of mRNAs have also been described (Chen et al., 2014; Eichhorn et al., 2016; Rissland et al., 2017; Subtelny et al., 2014; Wang et al., 2017; Winata et al., 2018), and global changes in the proteome have been documented (Baltz et al., 2012; Becker et al., 2018; Casas-Vila et al., 2017; Fabre et al., 2016; Gouw et al., 2009; Kronja et al., 2014; Peshkin et al., 2015; Stoeckius et al., 2014; Sysoev et al., 2016).

Relevant to the changes in the proteome is the ubiquitin-proteasome system, which is a highly conserved and widespread pathway for specific targeting of proteins for degradation (Komander and Rape, 2012; Ravid and Hochstrasser, 2008). This is accomplished through the E1-E2-E3 enzyme ubiquitination cascade, with the E3 ubiquitin ligase acting as the substrate-specificity factor, which transfers ubiquitin from an E2 ubiquitin-conjugating enzyme to specific target proteins (Pickart, 2001; Zheng and Shabek, 2017). Regulation of protein stability by the ubiquitin-proteasome system during the MZT has been noted in several studies. For example, MG132-directed inhibition of maternal protein degradation in mouse early zygotes delays ZGA (Higuchi et al., 2018). Also, in mouse, loss of an E3 ubiquitin ligase, RNF114, prevents development beyond the two-cell

This is an open access article under the CC BY-NC-ND license (http://creativecommons.org/licenses/by-nc-nd/4.0/).

stage (Yang et al., 2017). RNF114-directed ubiquitination and clearance of TAB1 permit nuclear factor-κB (NF-κB) pathway activation, although why this is necessary for the MZT is not known. In *C. elegans*, E3-ligase-directed clearance of the RBPs, OMA-1 and OMA-2, in the early embryo is crucial for the temporal coordination of ZGA (Du et al., 2015; Guven-Ozkan et al., 2008; Kisielnicka et al., 2018; Shirayama et al., 2006; Tsukamoto et al., 2017).

In *Drosophila melanogaster*, Smaug (SMG), a multifunctional RBP, is essential for both maternal mRNA degradation and ZGA (Benoit et al., 2009). SMG protein accumulates rapidly at the onset of embryogenesis, when the Pan gu (PNG) kinase complex abrogates translational repression of the *smg* and *Cyclin B* (as well as many other) mRNAs (Kronja et al., 2014b; Tadros et al., 2007; Vardy and Orr-Weaver, 2007). SMG binds target mRNAs through a stem-loop structure known as the SMG recognition element (SRE) (Aviv et al., 2003, 2006). Through these elements, SMG induces degradation and/or represses the translation of a large subset of the maternal transcripts (Chen et al., 2014; Semotok et al., 2005, 2008; Tadros et al., 2007; Zaessinger et al., 2006). SMG downregulates target mRNA expression through the recruitment of proteins that influence how these mRNAs interact with the mRNA decay and translation machineries. For example, SMG recruits the CCR4-NOT deadenylase complex to induce transcript degradation (Semotok et al., 2005) and the *Drosophila* miRNA Argonaute (AGO), AGO1, to repress mRNA translation (Pinder and Smibert, 2013). SMG acts in a complex with additional translational repressors, including the eIF4E-binding protein, Cup; the DEAD-box helicases, Maternal expression at 31B (ME31B) and Belle (BEL); and the FDF-domain protein, Trailer hitch (TRAL) (Götze et al., 2017; Jeske et al., 2011; Nakamura et al., 2001, 2004; Nelson et al., 2004; Wilhelm et al., 2000, 2003). PNG is required for the degradation of the Cup, TRAL, and ME31B repressors in early embryos (Wang et al., 2017), and at least one of these, TRAL, may be a direct substrate of PNG (Hara et al., 2018). SMG protein itself is rapidly degraded at the end of the MZT (Benoit et al., 2009; Siddiqui et al., 2012), but the mechanisms and functions of SMG clearance are unknown.

Leveraging the increasing sensitivity and measurement quality of multiplexed proteomics (Pappireddi et al., 2019; Sonnett et al., 2018), we present here a quantification of the developmental proteome of the *Drosophila* embryo. We show that the embryonic proteome represents over half of the protein-coding capacity of the genome, and thus is more than 40% larger than previously defined (Casas-Vila et al., 2017). We highlight a distinct cluster of proteins, comprising 2% of the maternally contributed embryonic proteome, that is highly expressed at the beginning of the MZT, but then rapidly degraded. This cluster includes SMG, Cup, TRAL, and ME31B. Focusing on these four repressors, we find that degradation of Cup, TRAL, and ME31B begins early and continues throughout the MZT, whereas SMG is degraded more abruptly and later, toward the end of the MZT. We identify two distinct E3 ubiquitin ligase complexes that target clearance of these proteins through the ubiquitin proteasome: the C-terminal to Lis1 Homology (CTLH) complex, which is homologous to the yeast Gid complex (Francis et al., 2013; Liu and Pfirrmann, 2019), targets Cup, TRAL, and ME31B; and the Skp/Cullin/F-box-containing (SCF) complex (Ho et al., 2006) targets SMG. We then engineer a stable version of the SMG protein that does not undergo degradation at the end of the MZT and show that persistent SMG downregulates zygotic re-expression of a subset of its maternal targets. Thus, clearance of SMG is necessary for this aspect of the MZT.

RESULTS

Definition and Dynamics of the Embryonic Proteome

We performed quantitative complement tandem mass tag (TMTc+) mass spectrometry (MS) (Sonnett et al., 2018) on the proteome of embryos at three stages that encompass the MZT, as well as at two later stages: (1) early syncytial blastoderm, prior to ZGA; (2) early nuclear cycle 14 (NC14) during blastoderm cellularization, after high-level ZGA; (3) germ-band extension, representing the end of the MZT; (4) germ-band retraction, representing mid-embryogenesis; and (5) tracheal filling, shortly before the end of embryogenesis (Table S1). We chose TMTc+ for this analysis because, in comparison with label-free methods, it generates data with higher measurement precision and overcomes the "missing value" problem (Pappireddi et al., 2019). TMTc+ also eliminates ratio compression, which is a common problem in other multiplexed proteomics approaches (Pappireddi et al., 2019; Sonnett et al., 2018; Ting et al., 2011). Importantly, due to the employed multiplexed proteomics approach, low signal in a condition is easy to interpret as low protein abundance. This is a major advantage over label-free measurements (for example, Casas-Vila et al., 2017) in which absence of signal could be caused by low abundance or because the mass spectrometer randomly did not detect the protein of interest (Pappireddi et al., 2019). We used BACIQ (Peshkin et al., 2019) to assign confidence to the relative expression of proteins at every stage (Table S1).

In total, we detected 7,956 unique proteins encoded by 7,683 genes (Table S1), representing 55% of the protein-coding genome (7,683/13,918 per FlyBase Release 6.03) (Matthews et al., 2015). We captured 97% of previously identified embryonically expressed proteins (5,186/5,359 genes) (Casas-Vila et al., 2017), as well as proteins encoded by an additional 2,294 genes (Figure 1A). This increases the size of the embryonic proteome by 43%. The newly detected proteins are significantly less abundant than those reported previously (Wilcoxon rank-sum test, $p < 10^{-4}$; Figure 1A).

To reveal classes of proteins with distinct expression dynamics during and after the MZT, we carried out k-means clustering of relative protein expression (Figure 1B; Table S1). A majority (65%) of proteins were present throughout the MZT and later embryogenesis, undergoing less than 2-fold increases or decreases in relative levels over the time course (clusters 1 and 2: 2,607 and 2,406 proteins, respectively). These either represent stable maternally encoded proteins, which are predominantly already deposited in the egg, similar to what has been observed in frog embryos (Peshkin et al., 2015), or proteins whose rates of synthesis and degradation are similar, thereby resulting in relatively constant levels (Kronja et al., 2014a). Proteins in clusters 3, 4, and 5 (1,123; 887; and 779 proteins, respectively)

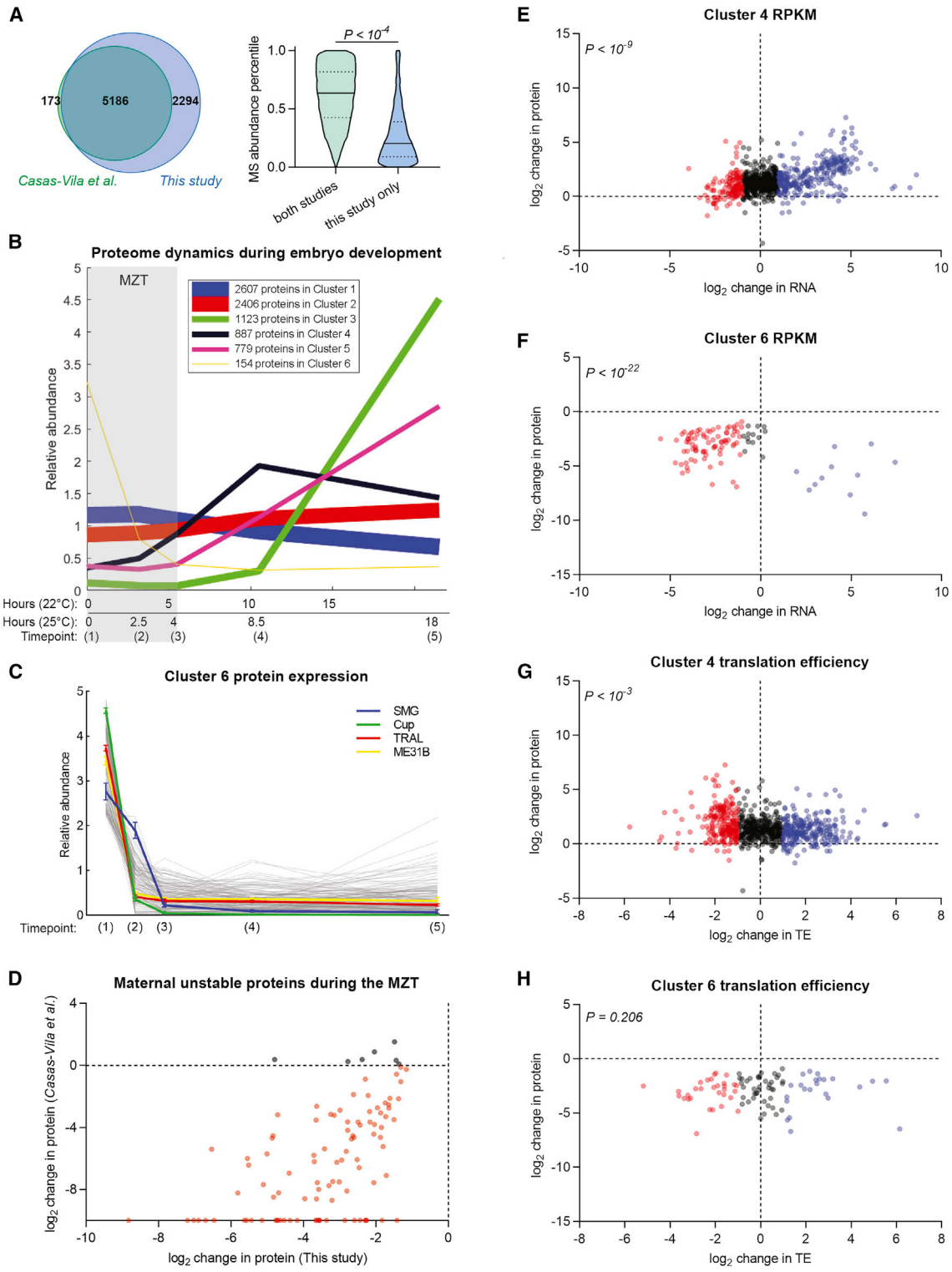

Figure 1. The *Drosophila* Proteome Is Dynamic during Embryogenesis

(A) Venn diagram comparing the previously reported embryonic proteome (Casas-Vila et al., 2017) with that defined in this study. Our methods captured 97% of the genes reported in the previous study and proteins encoded by an additional 2,294 genes. These additional proteins rank significantly lower in abundance than those reported in both studies. A small number of proteins that mapped to multiple genes were excluded from this analysis.

(legend continued on next page)

underwent significant increases in distinct waves: proteins in cluster 4 increased in levels during the MZT, reaching a peak at mid-embryogenesis and then declining somewhat thereafter. Proteins in cluster 5 increased in levels after the MZT and continued to rise throughout the rest of embryogenesis. Proteins in cluster 3 increased in levels at mid-embryogenesis and continued to increase thereafter. Strikingly, there was only one cluster that underwent a significant decrease in relative levels: 154 proteins were highest at the first time point and rapidly decreased to very low relative levels by the end of the MZT (cluster 6). Several members of cluster 6 have previously been shown to be cleared by the end of the MZT; examples include String (Edgar et al., 1994), Twine (Farrell and O'Farrell, 2013), BIGH1 (Pérez-Montero et al., 2013), PNG (Fenger et al., 2000), and Plutonium (Elfring et al., 1997).

Gene Ontology (GO) term analysis was conducted on each of the six clusters using the DAVID bioinformatics resource (Huang et al., 2009a, 2009b) (Table S2). Cluster 1 showed enrichment for terms related to the ubiquitin-proteasome system, as well as core biological processes, such as DNA replication and cell division. Cluster 2 was enriched for terms related to core components of mitochondrial function, endoplasmic reticulum (ER) and Golgi, transcription, splicing, and translation. Enrichment of clusters 1 and 2 for core cellular and molecular functions is consistent with the constant requirement for these components throughout development.

Cluster 4 was enriched for terms related to chromatin, sequence-specific DNA binding, transcriptional regulation, cell fate specification, and morphogenesis, consistent with the fact that ZGA is known to be required to produce transcription factors that specify cell fate and pattern starting at the cellular blastoderm stage (reviewed in Vastenhouw et al., 2019). Cluster 5 was enriched for terms related to cell adhesion and several morphogenetic processes (tube formation, heart, neuromuscular junction), consistent with the sculpting of tissues and organs after the MZT. Cluster 3 was enriched for terms related to chitin production and secretion, myogenesis, and synaptogenesis, consistent with a role for these proteins during the final stages of embryonic development and the secretion of the larval cuticle prior to hatching from the egg.

Cluster 6 was unusual in that relative expression was highest at the earliest stage of embryogenesis, following which its proteins were rapidly degraded to low levels by the end of the MZT (Figures 1B and 1C). A previous study of the embryonic proteome detected 104 of these 154 proteins (Casas-Vila et al., 2017). We compared the change in level of these proteins in the two datasets and found that 93% (97/104) were depleted in both datasets (Figure 1D). The degradation of only a small fraction of maternally loaded proteins stands in striking contrast with maternally loaded mRNA species, two-thirds of which are degraded by the end of the MZT (Thomsen et al., 2010).

Cluster 6 proteins must be either largely maternally supplied and already present in the oocyte, or rapidly synthesized from maternal mRNAs after egg activation or fertilization; we refer to them as "maternal" proteins. This cluster showed enrichment for GO terms related to the eggshell, as well as cytoplasmic ribonucleoprotein (RNP) granules (defined as non-membranous macromolecular complexes containing proteins and mRNAs), germ plasm, and germ cell development (Table S2). Because these RNP components are present during the first phase of the MZT, when gene expression is regulated primarily post-transcriptionally, it is plausible that they participate in these processes. Indeed, four components of the SMG-mediated repressor complex, SMG, Cup, TRAL, and ME31B, belong to cluster 6 (Figure 1C). These and several other RBPs in cluster 6 are known to have important functions in post-transcriptional regulation during the MZT.

To determine whether proteins in cluster 6 share an amino acid sequence motif that may provide insight into the mechanisms regulating their precise temporal degradation, we used the Multiple Em for Motif Elicitation (MEME) tool through The MEME Suite (http://meme-suite.org/) (Bailey and Elkan, 1994). Using cluster 1 proteins as a negative set, we found enrichment for several low-complexity motifs in cluster 6, notably poly-alanine and poly-glutamine tracts (Figure S1A). RBPs are known to be rich in intrinsically disordered regions (Wang et al., 2016), and

(B) k-means clustering (k = 6) for 7,956 quantified proteins through embryogenesis. Embryos were aged to five developmental time points at 22°C. The equivalent developmental times at 25°C for each sample are indicated on the x axis. The first three samples cover the MZT (gray box).
(C) Expression profile of individual cluster 6 proteins (gray lines) through embryogenesis reveals the maternal nature of these proteins and their rapid clearance during the MZT, restricting their expression mostly to the early embryo. Profiles of SMG, Cup, TRAL, and ME31B are shown in color, highlighting the later timing of SMG's degradation relative to its co-repressors. Error bars indicate upper and lower limit of relative expression with a 95% Bayesian confidence interval at each time point.
(D) Scatterplot comparing the degradation of cluster 6 proteins during the MZT in this study with that previously reported (Casas-Vila et al., 2017). 104 of our 154 cluster 6 proteins were also found in that study. Almost all cluster 6 proteins that decreased in expression during the MZT (time point 3/time point 1) showed a similar decrease in the previous report (4–5 h/0–1 h) (plotted in red). Note that proteins that decreased to undetectable levels by 4–5 h are plotted on the x axis.
(E and F) Scatterplot of change in RNA expression (reads per kilobase of transcript, per million mapped reads [RPKM], 3–4 h/0–1 h) (Eichhorn et al., 2016) versus change in protein expression (time point 3/time point 1) for dynamic proteins during the MZT. Genes corresponding to RNA with ≥2-fold decrease in expression are plotted in red; ≥2-fold increase in expression are plotted in blue.
(E) Proteins that increased in expression during the MZT (cluster 4) showed a significant correspondence with ≥2-fold increase in their transcript expression ($p < 10^{-9}$).
(F) Proteins that decreased in expression (cluster 6) showed a significant correspondence with ≥2-fold decrease in their transcript expression during the MZT ($p < 10^{-22}$).
(G and H) Scatterplot of change in translational efficiency (TE, 3–4 h/0–1 h) (Eichhorn et al., 2016) versus change in protein expression (time point 3/time point 1) for dynamic proteins during the MZT. Genes corresponding to RNA with ≥2-fold decrease in TE are plotted in red; ≥2-fold increase in TE is plotted in blue.
(G) Cluster 4 proteins showed a significant correspondence with ≥2-fold increase in TE of their transcripts ($p < 10^{-3}$).
(H) Cluster 6 proteins were not associated with significant changes in TE of their transcripts (p = 0.206).
Fisher's exact test was performed for (E)–(H). See also Figure S1 and Tables S1 and S2.

there is enrichment of RBPs in cluster 6. To overcome this possible bias, we re-ran MEME using as a negative set only the 394 annotated RBPs and RNP-associated proteins in cluster 1 and, again, found enrichment for glutamine-rich motifs (Figure S1B). This motif was found in 34 of the 154 cluster 6 proteins and, thus, is unlikely, by itself, to explain degradation of the entire cluster. We conclude that there is no single, simple protein motif that distinguishes the rapidly degraded maternal cluster 6 proteins from co-expressed maternal proteins that are stable through the MZT.

Dynamics of the Proteome Relative to the Transcriptome and Translatome during the MZT

We next compared the relative changes in the proteome (this study) with those previously identified for either the RNA population ("transcriptome") or for ribosome-associated mRNAs ("translatome") (Eichhorn et al., 2016) at equivalent time points across the MZT. We focused on cluster 4 (newly synthesized during the MZT) and cluster 6 (degraded during the MZT). A previous study that compared the embryonic proteome and transcriptome excluded almost all proteins in cluster 6 from their analysis because of these proteins' narrow expression window (Becker et al., 2018).

A significant proportion of mRNAs encoding proteins in cluster 4 underwent increases in RNA levels and ribosome association at comparable time points (Fisher's exact test, $p < 10^{-9}$ and $p < 10^{-3}$, respectively; Figures 1E and 1G). However, whereas a significant proportion of the cluster 6 unstable maternal proteins underwent a concomitant decrease in cognate mRNA levels (Fisher's exact test, $p < 10^{-22}$; Figure 1F), there was no correlation with changes in ribosome association (Fisher's exact test, $p = 0.206$; Figure 1H). This last result is consistent with the fact that some of the cluster 6 proteins, such as SMG, are synthesized during the MZT rather than during oogenesis; thus, their cognate mRNAs exhibit high ribosome association despite the fact that their encoded proteins are subsequently rapidly cleared.

In summary, the subset of proteins that undergoes extensive increases in levels during the MZT (cluster 4) shows parallel increases in both mRNA level and translation efficiency. In contrast, the subset that decreases rapidly during the MZT (cluster 6) undergoes parallel decreases in levels of cognate mRNAs, but not translation efficiency.

Maternal Ribonucleoprotein Complex Components Are Degraded during the MZT

A closer examination of the cluster 6 RNP granule proteins revealed different decay profiles during the MZT. Of the 17 RBPs and RNP-associated proteins in cluster 6, several were cleared from the embryo very rapidly and were depleted by the second time point. These included Cup, TRAL, and ME31B (highlighted in Figure 1C), as well as BicaudalC, Swallow, Wispy, Cp7Fa, and Spargel. Others underwent most of their degradation between the second and third time points, including SMG (shown in Figure 1C), Vasa, Oskar, and Tudor. Seven of the 17 RBPs contained one or more of the MEME-identified polyalanine or polyglutamine motifs described above. Note that not all maternally loaded RBPs fell into cluster 6; several were stable and fell into clusters 1 or 2 (e.g., Brain tumor, Pumilio, Rasputin, Egalitarian, BEL, PABP; see Table S1).

To verify the results of the MS and to assess the dynamics of SMG, Cup, TRAL, and ME31B expression at higher temporal resolution, we carried out western blot analysis of extracts from embryos collected in overlapping 30-min intervals through the first 6 h of embryogenesis (Figures 2A and S2). Cup, TRAL, and ME31B are maternally supplied proteins with highest expression at the onset of embryogenesis (Casas-Vila et al., 2017; Sysoev et al., 2016; Wang et al., 2017). Our analysis showed that these proteins decline in parallel, coincident with degradation of their cognate transcripts (Wang et al., 2017). Degradation started early, even before 1 h, and its completion at approximately 2.5 h coincided with early NC14. Whereas Cup fell below the limit of detection, TRAL and ME31B persisted at reduced levels (nearly 10% based on quantification of the western blot). Disappearance of Cup and persistence of low levels of ME31B and TRAL were also visible in the MS analysis (Figure 1C). In contrast with these three proteins, SMG protein expression was low at the onset of embryogenesis and peaked at about 1 h, corresponding with rapid translational derepression of the maternally loaded *smg* transcripts upon egg activation (Tadros et al., 2007). SMG then persisted at more or less constant levels before undergoing precipitous degradation between about 2.5 and 3 h (Benoit et al., 2009; Casas-Vila et al., 2017), coinciding with blastoderm cellularization and high-level ZGA. Disappearance of SMG was nearly complete, as judged both from western blotting and our MS analysis (Figures 1C, 2A, and S2; Table S1). Two additional proteins associated with the *nanos* repressor complex (Götze et al., 2017; Jeske et al., 2011) were also assessed: the DEAD-box helicase, BEL, and the cap-binding protein, eIF4E. Levels of BEL remained fairly constant (67% remained at 4 h), whereas eIF4E gradually decreased in abundance but was clearly detectable throughout the time course (19% remained after 4 h). The results of our western blot analyses of BEL and eIF4E are consistent with both our own MS data and published datasets (Casas-Vila et al., 2017; Sysoev et al., 2016; Wang et al., 2017).

Previous studies have shown that the clearance of SMG protein from the embryo depends on ZGA (Benoit et al., 2009). To determine the role of ZGA in the degradation of Cup, TRAL, and ME31B, we analyzed their expression (as well as that of SMG, as a control) in activated, unfertilized eggs, which carry out maternally directed post-transcriptional and post-translational processes, but do not undergo transcriptional activation (Bashirullah et al., 1999; Page and Orr-Weaver, 1997; Tadros et al., 2003). Embryo extracts were collected from wild-type mated and unmated females in 1-h intervals over 4 h, and expression of the RBPs was assayed by western blotting (Figure 2B). The clearance of Cup, TRAL, and ME31B was unaffected in unfertilized eggs, indicating that their degradation is not dependent on ZGA. In contrast and as expected, SMG protein was stable in unfertilized eggs (Benoit et al., 2009). Thus, Cup-TRAL-ME31B and SMG differ both in the timing of their degradation and in whether they require zygotically synthesized gene products to accomplish this process.

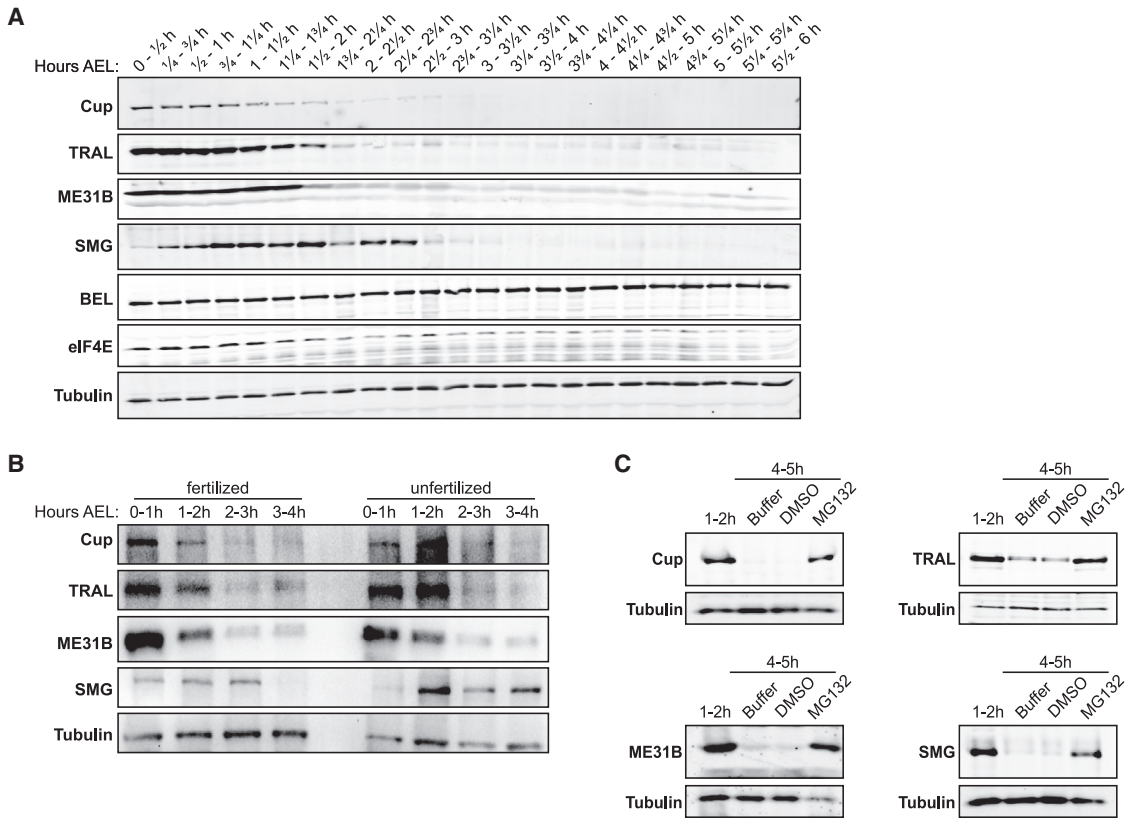

Figure 2. SMG, Cup, TRAL, and ME31B Are Degraded at Distinct Times during the MZT through the Ubiquitin-Proteasome System

(A) Developmental western blot of wild-type embryos collected in 30-min time windows and aged at 15-min intervals over the first 6 h after egg lay (AEL). Cup, TRAL, and ME31B are notably decreased by around 1.5 h AEL, whereas SMG levels increase in the early embryo and are subsequently cleared by about 2.5 h AEL. BEL and eIF4E are present for the duration of the time course. Tubulin was probed as a loading control. See Figure S2 for quantification.

(B) Developmental western blot of wild-type embryos collected over the first 4 h of embryogenesis from mated females (fertilized) and unmated females (unfertilized). Degradation of Cup, TRAL, and ME31B are unaffected in unfertilized eggs, whereas SMG protein fails to be degraded by 3–4 h AEL.

(C) Western blots of 1- to 2-h-old embryos that were permeabilized and incubated for 3 h in buffer, DMSO control, or 100 μM MG132 and aged to 4–5 h AEL. All four RBPs shown are stabilized by MG132 treatment.

See also Figures S2 and S3.

Degradation of the Repressors Is Regulated by the Ubiquitin-Proteasome System

To determine whether clearance of SMG, Cup, TRAL, and ME31B occurs via the ubiquitin-proteasome system, we inhibited the proteasome in developing embryos using the small molecule, MG132. 1- to 2-h-old embryos were permeabilized (Rand et al., 2010) and incubated with either MG132 or control buffer, then allowed to develop for a further 3 h. Western blots on controls showed that SMG, Cup, TRAL, and ME31B were degraded as expected. Strikingly, treatment with 100 μM MG132 resulted in stabilization of all four RBPs (Figure 2C).

If the ubiquitin-proteasome system indeed targets these proteins for degradation, it should be possible to identify specific sites of ubiquitination. In MS analysis of tryptic protein digests, ubiquitination is visible as a lysine to which the two C-terminal glycine residues of ubiquitin are attached; often, the modified lysine residue is not cleaved by trypsin. A reanalysis of our previous MS data (Götze et al., 2017) revealed ubiquitination signatures in all four repressors (Table S3).

Together these data support a role for the ubiquitin-proteasome in clearance of SMG, Cup, TRAL, and ME31B proteins during the MZT.

Two Distinct Ubiquitin Ligase Complexes Interact with the Repressors

To identify the specific E3 ligases that regulate degradation of the repressors during the MZT, we performed immunoprecipitation followed by mass spectrometry (IP-MS) from transgenic embryos expressing FLAG-tagged SMG protein and used Significance Analysis of Interactome (SAINT) to characterize interactors of SMG (Choi et al., 2011). As expected, Cup, TRAL, and ME31B, as well as BEL and eIF4E, were highly enriched in FLAG-SMG IPs relative to control IPs, placing them among the top interactors (Figure 3A; Table S4) and recapitulating the known repressive complex (Götze et al., 2017; Jeske et al., 2011). We note that these RBPs were also detected, albeit at much lower levels, in our control IPs, likely as a result of some level of nonspecific interaction exacerbated by the very high expression levels of these RBPs at this stage of embryogenesis.

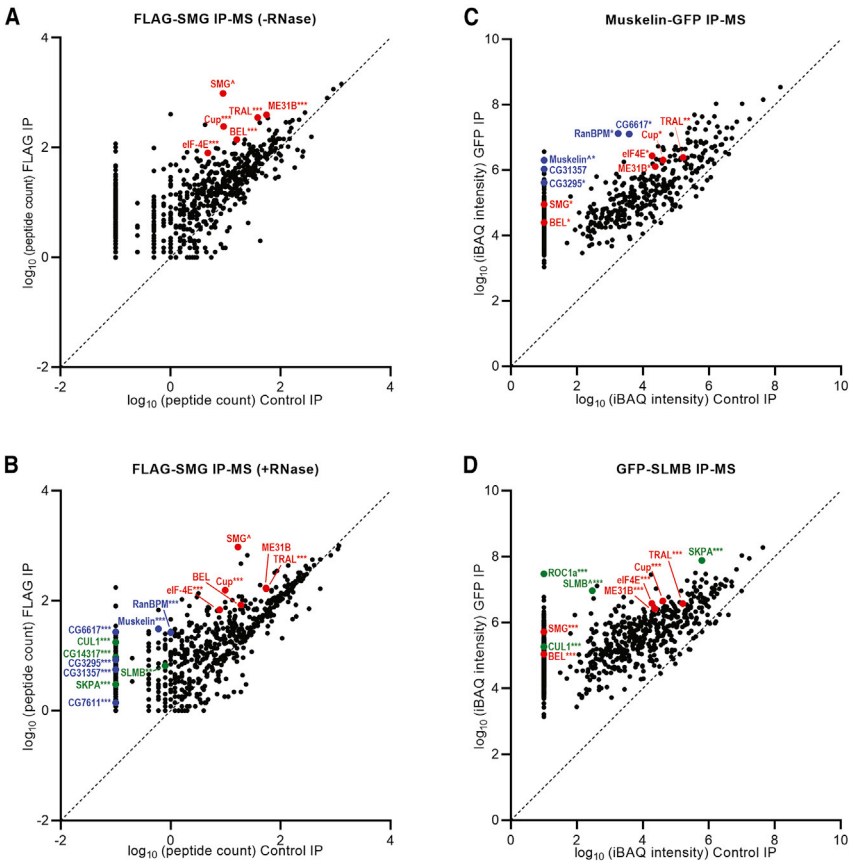

Figure 3. SMG Interacts with Repressor RBPs and Two Distinct E3 Ubiquitin Ligase Complexes

(A and B) FLAG IP-MS of 0- to 3-h embryo lysate collected from transgenic flies expressing FLAG-SMG and homozygous for the deletion allele *smg*^{47}. A combination of Protein A control IP and FLAG IP from non-transgenic embryo lysate was used as control. Average spectral counts are plotted for proteins detected at ≥1 in FLAG-SMG IP on average across at least four biological replicates. Significance of interactors was analyzed using SAINT and annotated for proteins of interest: *p ≤ 0.1, **p ≤ 0.05, ***p ≤ 0.001, ^Bait (significance of interaction not applicable).

(A) In the absence of RNase A, SMG exhibited significant interactions with the co-repressive complex: Cup, TRAL, ME31B, BEL, and eIF4E (red).

(B) In the presence of RNase A, SMG retained significant interactions with its co-repressors Cup and TRAL, but not significantly with ME31B (red). The IP also captured RNA-independent interactions with two E3 ubiquitin ligase complexes: the CTLH complex (blue: Muskelin, RanBPM, CG6617, CG3295, CG31357, and CG7611) and the SCF complex (green: CUL1, SKPA, CG14317, and SLMB).

(C and D) GFP IP-MS of 0- to 2-h lysate from embryos expressing either Muskelin-GFP or GFP-SLMB. GFP IP from non-transgenic embryo lysate was used as control. Average iBAQ intensities (Cox and Mann, 2008) for proteins across three biological replicates are plotted. Significance of enrichment in IP versus control was analyzed for each interactor using Student's t test and annotated for proteins of interest: *p ≤ 0.1, **p ≤ 0.05; ***p ≤ 0.01, ^Bait.

(C) Muskelin-GFP interacts with the RBPs (red) and other members of the CTLH complex (blue).

(D) GFP-SLMB interacts with the RBPs (red) and other members of the SCF complex (green).

Proteins not detected in control IPs were assigned an average spectral count of 0.1 (A and B) or an iBAQ value of 10 (C and D) to avoid log(0); these small values were at least 2-fold less than the lowest detected values across all experiments. See also Tables S4 and S5.

In addition, we captured RNA-independent interactions with several members of two distinct multi-subunit E3 ubiquitin ligase complexes: the SCF complex and the CTLH complex (Figure 3B; Table S4). SCF complex components that were identified included core components such as SKPA (Skp) and CUL1 (Cullin), as well as SLMB and CG14317 (F-box proteins) (Ravid and Hochstrasser, 2008), whereas the CTLH complex was represented by all of the characterized *Drosophila* subunits (Francis et al., 2013): RanBPM, Muskelin, CG6617, CG3295, CG7611, and CG31357 (Figure 3B; Table S4). Detection of the CTLH complex confirmed earlier data (Götze et al., 2017).

To verify the interaction of these two E3 ligase complexes with the repressors, we performed an independent set of reciprocal IP-MS experiments using embryos expressing GFP-SLMB or Muskelin-GFP. Muskelin-GFP IPs from RNase-treated extracts were highly enriched for additional members of the CTLH complex and for the four repressors (Figure 3C; Table S5). Variation in the amount of Muskelin IPed between biological replicates resulted in the enrichment of several CTLH subunits having significance only at $p < 0.1$ (Figure 3C). GFP-SLMB pull-downs from RNase-treated extracts captured highly significant enrichment relative to control ($p < 0.01$) for additional subunits of the SCF complex, as well as the four repressors (Figure 3D; Table S5). The association of all four repressors with both E3 ligase complexes presumably reflects the formation of stable repressor complexes.

Degradation of Cup, TRAL, and ME31B Is Directed by the CTLH E3 Ubiquitin Ligase

The CTLH complex has previously been shown to copurify with the SMG-Cup-TRAL-ME31B repressive complex (Götze et al., 2017), but the functional significance of this interaction has not been elucidated; neither has a role for the CTLH been identified in any other biological process in *Drosophila*. The SCF complex has been implicated in multiple processes, including the cell cycle, control of cell polarity, cell-cell signaling, and the germ plasm (see, for example, Morais-de-Sá et al., 2013; Noureddine et al., 2002; Wojcik et al., 2000), but a possible role during the MZT has not been studied.

To investigate the role of the SCF and the CTLH E3 ubiquitin ligase complexes in degradation of the repressors during the MZT, we performed maternal RNAi knockdown experiments for several core members of the SCF and CTLH complexes. Embryos were collected at 1-h intervals from female flies with

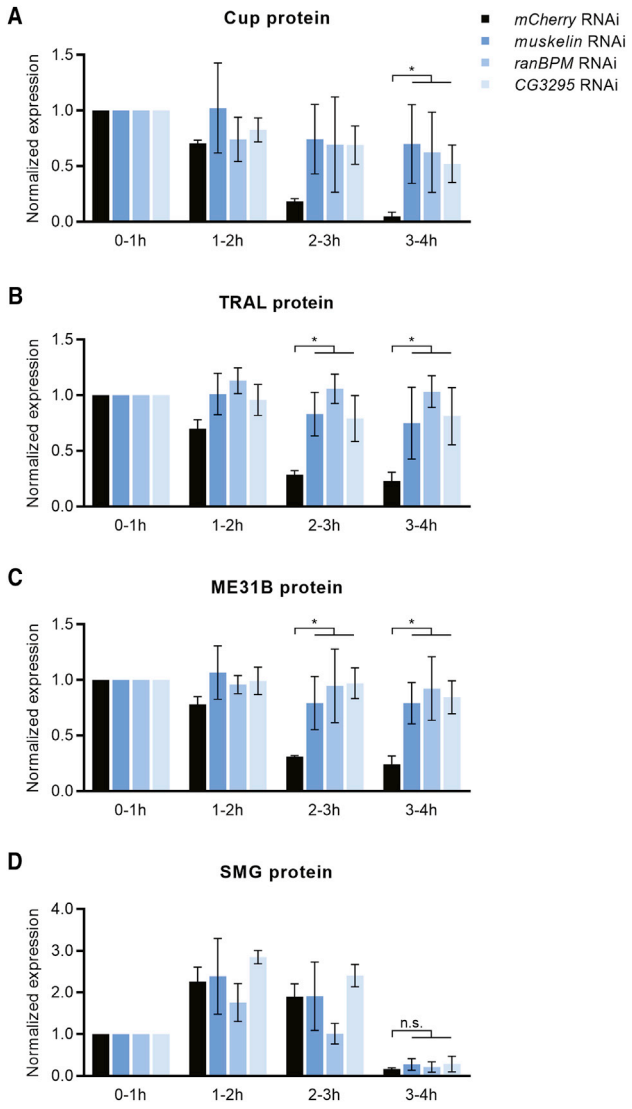

Figure 4. The CTLH Complex Directs the Degradation of Cup, TRAL, and ME31B, but Not SMG

(A–C) Quantified developmental western blots of RBP expression. Embryos were collected from maternal knockdown of CTLH complex members over the first 4 h AEL. Knockdown of *muskelin*, *ranBPM*, and *CG3295* each independently resulted in significant stabilization of Cup (A), TRAL (B), and ME31B (C) relative to control *mCherry* knockdown.

(D) SMG protein degradation was unaffected by knockdown of the CTLH complex.

*$p < 0.05$; n = 3; error bars indicate SD, Student's t test. n.s., not significant. Knockdown was confirmed by qRT-PCR (Figure S3). See also Figures S4 and S5.

germline knockdown, and expression of SMG, Cup, TRAL, and ME31B was assessed by western blot over the first 4 h of embryogenesis. Knockdown was confirmed in these embryos by qRT-PCR and, in the case of SLMB, also by western blot (Figures 4, 5, S3, and S6).

Individual maternal knockdown of the CTLH complex members Muskelin, RanBPM, or CG3295 resulted in stabilization of Cup, TRAL, and ME31B proteins (Figures 4A–4C), whereas SMG protein degradation was unaffected (Figure 4D). In these experiments, knockdown of the CTLH complex components also resulted in a delay in the degradation of *cup, tral*, and *me31B* transcripts (Figure S4). DAPI staining of the RNAi embryos revealed a developmental delay in a subset (about 20%). To eliminate the possibility that developmentally delayed or arrested embryos contributed to repressor protein "persistence," we visualized embryo development live under halocarbon oil and picked embryos at three specific developmental stages during the MZT for analysis: stage 2 (0.5–1 h of embryogenesis), stage 5b (2.5 h of embryogenesis), and stage 7b (3 h of embryogenesis). Developmentally delayed or abnormal embryos were thus excluded by this method. Knockdown of any of the three members of the CTLH complex led to nearly complete stabilization of Cup, TRAL, and ME31B through to stage 7b, whereas in controls, all three proteins were degraded by stage 5b (Figure S5). qRT-PCR quantification of mRNA expression in these staged embryos showed that *cup* mRNA was cleared from the embryo by stage 7b both in knockdown and in control embryos. This result excludes new synthesis as the reason for the persistence of Cup under conditions of CTLH complex knockdown, thus providing strong evidence that the CTLH complex is required for degradation of the Cup protein (Figure S5). However, *tral* and *me31B* transcripts were partially stabilized in stage 7b embryos (Figure S5); thus, we cannot rule out the possibility that translation from their stabilized cognate transcripts contributes in part to the persistence of TRAL and ME31B protein. Either way, it is clear that the CTLH plays a key role in clearance of Cup and, likely, also TRAL and ME31B, but not in clearance of SMG.

Degradation of SMG Is Directed by the SCF E3 Ubiquitin Ligase

In contrast with the CTLH complex, we found that maternal knockdown of the SCF complex members CUL1, SKPA, or SLMB had no effect on Cup, TRAL, and ME31B expression but resulted in stabilization of SMG protein (Figure 5). Furthermore, we confirmed by qRT-PCR that degradation of *smg* mRNA, which is coincident with SMG protein's clearance, was unaffected in these embryos (Figure S7). Thus, persistence of SMG in the absence of the SCF E3 ligase complex must have been a result of protein stabilization. Finally, to exclude the possibility that stabilization of SMG was a result of a developmental delay resulting from these knockdowns, we performed immunostaining of SMG in the RNAi embryos. Whereas SMG normally disappears from the bulk cytoplasm of embryos prior to gastrulation, in knockdown of core members of the SCF complex, we found gastrulating embryos ubiquitously staining for high levels of SMG protein (Figure S7).

Taken together, these data provide strong evidence that the SCF E3 ubiquitin ligase complex regulates degradation of SMG protein at the end of the MZT, whereas the CTLH complex directs degradation of Cup, TRAL, and ME31B.

Temporal Regulation of the E3 Ligase Complexes

What determines the timing of E3 ligase complex action? We assessed the dynamics of CTLH and SCF subunits in our TMTc+ MS data and found that, with the exceptions described below,

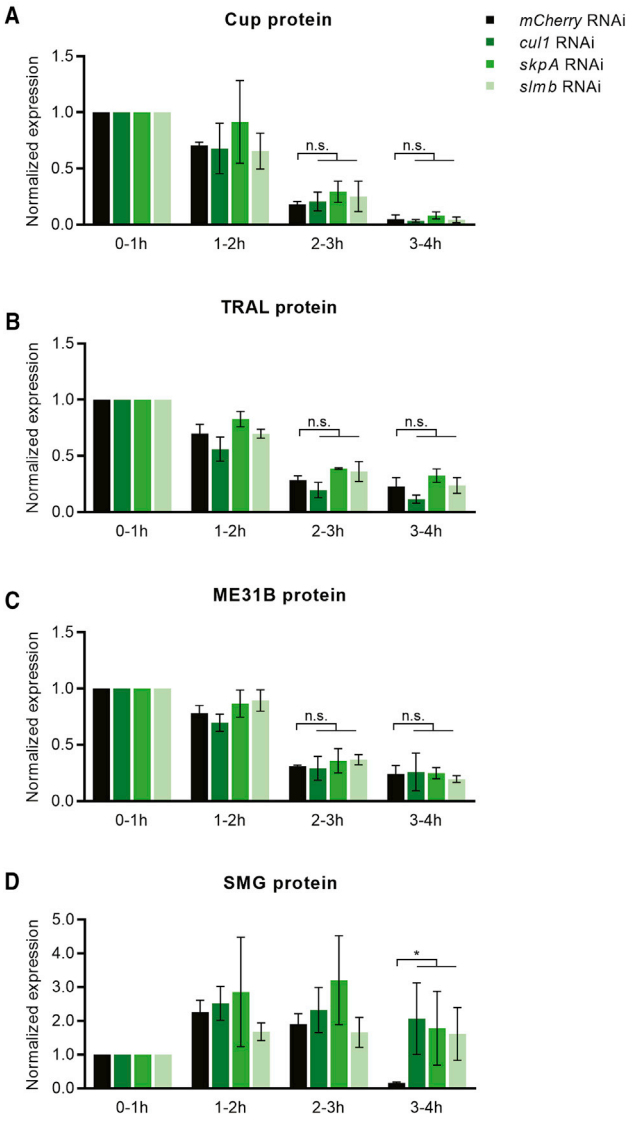

Figure 5. The SCF Complex Directs the Degradation of SMG, but Not Cup, TRAL, and ME31B

(A–C) Quantified developmental western blots of RBP expression. Embryos were collected from maternal knockdown of SCF complex members over the first 4 h AEL. Cup (A), TRAL (B), and ME31B (C) protein degradation were unaffected by knockdown of the SCF complex.

(D) Knockdown of *cul1*, *skpA*, and *slmb* each independently resulted in significant stabilization of SMG protein relative to control *mCherry* knockdown. *$p < 0.05$; n = 3; error bars indicate SD, Student's t test. n.s., not significant. Knockdown was confirmed by qRT-PCR (Figure S6). See also Figure S7.

the subunits detected (CTLH: RanBPM, CG3295, CG6617, CG7611, CG31357; SCF: CUL1, SKPA, ROC1a, SLMB) were present throughout embryogenesis (Figure 6). These results are consistent with cluster 1 proteins showing enrichment for the GO term "ubiquitin-proteasome system."

In contrast with the other CTLH subunits, the relative level of Muskelin decreased rapidly during the MZT (Figure 6A), consistent with previous MS results (Casas-Vila et al., 2017). We confirmed this expression profile by western blotting of GFP-tagged Muskelin and comparison with endogenous CG3295 (Figure 6B). Furthermore, our re-analysis of previously published data (Götze et al., 2017) revealed that Muskelin is ubiquitinated in early embryos (Table S3). The role of Muskelin in the function of the CTLH complex is unknown; however, these data are consistent with the possibility that the dynamics of Muskelin clearance might restrict CTLH function to the early phase of the MZT, coinciding with the timing of Cup, TRAL, and ME31B degradation.

For the SCF complex, our TMTc+ MS showed that the CUL1, SKPA, ROC1a, and SLMB subunits were present at relatively constant levels throughout embryogenesis (Figure 6C), and western blots confirmed that SLMB is expressed throughout the MZT (Figure 6D). The F-box subunit confers substrate specificity to the SCF complex, and SLMB is one of two F-box proteins that we found to interact with SMG by IP-MS (Figure 3B). Strikingly, the second F-box protein, CG14317, displayed a highly unusual expression pattern: the CG14317 mRNA is absent at the beginning of embryogenesis, is zygotically expressed, peaking during the late MZT, and then drops precipitously (Brown et al., 2014; Graveley et al., 2011). The mRNA is not detected at any other stage of *Drosophila* development, neither is it found in any tissue or cell line that has been profiled (http://flybase.org/reports/FBgn0038566). Both our (Figure 6C) and previously published MS data (Casas-Vila et al., 2017) showed that the CG14317 protein follows an almost identical expression pattern to that of its cognate mRNA; thus, CG14317 is expressed when SMG protein degradation is triggered. Furthermore, degradation of SMG near the end of the MZT depends on zygotic transcription, and CG14317 mRNA and protein are produced zygotically. We speculate that CG14317 could serve as a timer for SCF action on SMG (see Discussion).

Persistent SMG Protein Downregulates Zygotic Re-expression of Its Target Transcripts

The SMG RBP contains a dimerization domain near its N terminus (Tang et al., 2007) and a SAM-PHAT RNA-binding domain toward the C terminus (Aviv et al., 2003, 2006). We produced transgenic fly lines expressing FLAG-p53-tagged SMG, either full-length ("FLAG-SMG") or missing the C-terminal 233 amino acids ("FLAG-SMG767Δ999") (Figure 7A). FLAG-SMG767Δ999 is deleted for two of the three ubiquitination sites detected in our MS (Table S3); the third site resides in the SAM-PHAT domain, just N-terminal to the deletion. The transgenes were under control of the endogenous *smg* gene's regulatory elements and, to avoid potential complications resulting from dimerization of transgenic FLAG-SMG with endogenous SMG, all assays were conducted in the smg^{47} null mutant background (Chen et al., 2014).

To assess whether the deletion reduced interaction with the SCF E3 ligase, we carried out IP-MS of FLAG-SMG and FLAG-SMG767Δ999. The deletion showed a striking reduction of interaction with the F-box proteins SLMB and CG14317 relative to full-length SMG (Table S4): whereas SLMB and CG14317 were readily detected for full-length FLAG-SMG, respectively, with SAINT scores of 1.0 (Bayesian false discovery rate [BFDR 0.0]) and 0.96 (BFDR 0.0), they were completely undetected in the FLAG-SMG767Δ999 IP-MS.

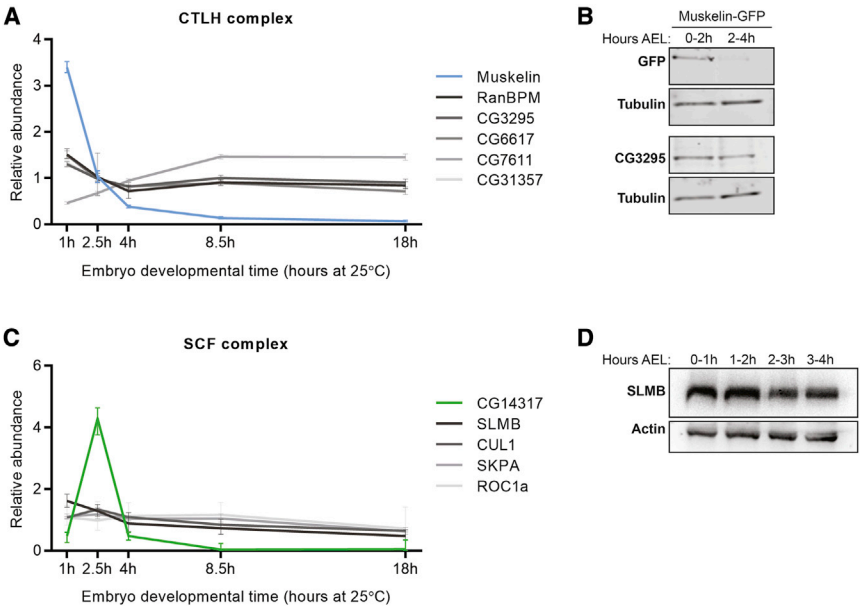

Figure 6. Subunits of the E3 Ligase Complexes Are Temporally Regulated during the MZT

(A) Expression of subunits of the CTLH complex captured in the developmental proteome. Error bars indicate the upper and lower limit of relative expression with a 95% Bayesian confidence interval at each time point. Most subunits have relatively constant levels throughout embryogenesis, whereas levels of Muskelin are highest at the first time point and then decrease rapidly.

(B) Western blot of embryos expressing Muskelin-GFP. Anti-GFP (top) confirmed rapid clearance of Muskelin-GFP from the embryo. Anti-CG3295 (bottom) confirmed its stable expression during the MZT.

(C) Expression of subunits of the SCF complex captured in the developmental proteome. Error bars are the same as in (A). Most subunits exhibit relatively constant levels throughout embryogenesis, whereas levels of the F-box subunit CG14317 increased rapidly during the MZT and then decreased very rapidly by the end of the MZT, with peak levels coinciding with degradation of SMG protein.

(D) Developmental western blot of control RNAi embryos, confirming the stable expression of SLMB during the MZT. Notably, the same blot shown here was used to confirm SLMB knockdown in Figure S6.

Next, we assessed the effect of the deletion on protein stability and found that truncation of SMG's C-terminal 233 amino acids led to stabilization of the protein throughout the MZT (Figure 7B). We conclude that the truncated SMG protein has significantly decreased SCF interactions, and that this correlates with failure to clear the protein at the end of the MZT.

This positioned us to study the effects of persistent SMG. SMG is known to target hundreds of maternal transcripts for degradation during the MZT (Chen et al., 2014; Tadros et al., 2007). A subset of these transcripts is re-expressed upon ZGA (Benoit et al., 2009; De Renzis et al., 2007; Thomsen et al., 2010). Given that the CCR4-NOT deadenylase complex, through which SMG is known to destabilize its target mRNAs, remains expressed at fairly constant levels throughout embryogenesis (cluster 1; also, see Temme et al., 2004), we hypothesized that persistent SMG protein may result in unintentional targeting of zygotically re-expressed SMG targets. To test this hypothesis, we compared transcript dynamics in *smg*^{47} mutant embryos expressing either full-length FLAG-SMG or FLAG-SMG767Δ999. Gene expression was assayed by qRT-PCR in 0- to 2.5-h-old embryos (representing the maternal phase of the MZT) and 2.5- to 5-h-old embryos (representing the zygotic phase of the MZT).

Embryos that lack SMG protein fail to undergo both maternal mRNA decay and ZGA (Benoit et al., 2009; Tadros et al., 2007). We, therefore, first carried out two control experiments to assess whether FLAG-SMG767Δ999 rescues these processes. One control focused on strictly zygotic transcripts that lack SMG binding sites (Benoit et al., 2009). We found that these were expressed at comparable (or even higher; Wilcoxon signed rank test, $p < 0.02$) levels for FLAG-SMG767Δ999 versus full-length FLAG-SMG, showing that FLAG-SMG767Δ999 rescues ZGA (Figure 7C). A second control analyzed degradation of SMG-bound maternal transcripts that are targeted by SMG but are not re-expressed zygotically (Chen et al., 2014; Tadros et al., 2007). We found that these were degraded in FLAG-SMG767Δ999 embryos, sometimes (*Frip84*, *FBXO11*, *Rpn2*, *Rpn7*) to even lower levels than in embryos expressing full-length SMG (Wilcoxon signed rank test, $p < 3 \times 10^{-3}$; Figure 7D). Thus, FLAG-SMG767Δ999 also rescues maternal mRNA decay. Finally, we assayed the expression of transcripts that met three criteria: (1) maternally supplied and degraded in a SMG-dependent manner (Tadros et al., 2007), (2) directly bound by SMG (Chen et al., 2014), and (3) zygotically re-expressed at high levels upon initiation of ZGA (Benoit et al., 2009). Strikingly, *smg*^{47} embryos expressing FLAG-SMG767Δ999 showed significantly lower zygotic expression of these transcripts when compared with *smg*^{47} embryos expressing full-length FLAG-SMG (Wilcoxon signed rank test, $p < 4 \times 10^{-3}$; Figure 7E).

We conclude that precise temporal regulation of SMG protein degradation at the end of the MZT is required to permit proper zygotic re-expression of transcripts with SMG binding sites.

DISCUSSION

Here we have shown that, in *Drosophila*, an extremely small subset of its maternal proteome is cleared during the MZT. This contrasts with the massive degradation of the maternal mRNA transcriptome that occurs during the MZT of all animals (reviewed in Vastenhouw et al., 2019). Previous studies in other animals have suggested that the maternal proteome may behave very differently from the maternal transcriptome during the MZT. For example, in *C. elegans*, a quarter of the transcriptome is

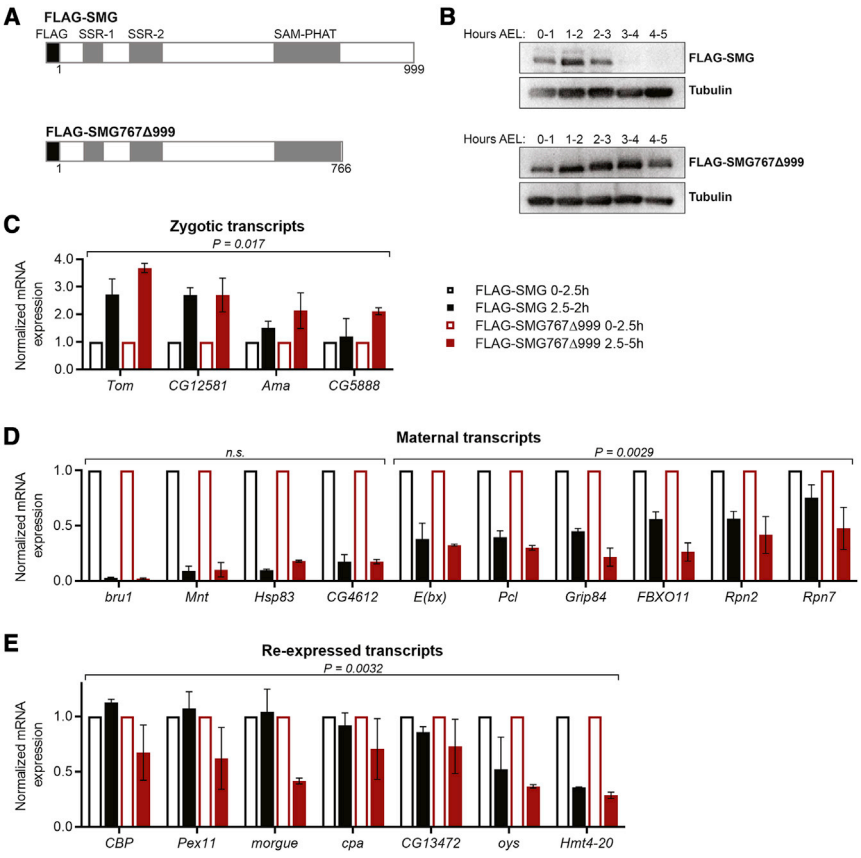

Figure 7. Persistent SMG Protein Downregulates Zygotic Re-expression of Its Target Transcripts

(A) Transgenic flies were generated expressing either FLAG-tagged full-length SMG or SMG767Δ999 truncated C-terminal to its SAM-PHAT RNA-binding domain. Transgenes were under the control of endogenous regulatory elements.

(B) Developmental western blots were performed on embryos collected from transgenic flies in the *smg*^{47} deletion mutant background. FLAG-SMG expression resembled that of endogenous SMG. SMG767Δ999 protein was stabilized and persisted through the MZT.

(C–E) Embryos were collected from the transgenic flies at two time points during the MZT, and gene expression was assayed by qRT-PCR.

(C) Expression of transcripts that depend on SMG for zygotic transcription was rescued by SMG767Δ999 to similar or higher levels than by full-length SMG. These transcripts are predicted not to be direct targets for SMG binding because they have low SRE scores (see STAR Methods).

(D) Degradation of SMG-bound target maternal transcripts was rescued by SMG767Δ999. Where transcripts were not completely degraded by FLAG-SMG, SMG767Δ999 persistence resulted in further degradation of these targets to significantly lower levels (rightmost six genes).

(E) SMG-target maternal transcripts that are re-expressed zygotically were significantly downregulated in their zygotic levels by persistence of SMG767Δ999. Wilcoxon signed rank test p values are shown for each gene group; two biological replicates for each gene; error bars indicate SD.

downregulated, whereas only 5% of the proteome shows a similar decrease (Stoeckius et al., 2014). In frog embryos, there is also a discordance between the temporal patterns of protein and mRNA (Peshkin et al., 2015).

The set of proteins cleared during the *Drosophila* MZT is enriched for RNP granule components. This is consistent with the importance of post-transcriptional processes during the first ("maternal") phase of the MZT and the possible need to downregulate these processes upon ZGA and the switch to zygotic control of development. By focusing on a subset of these RNP components, which function as post-transcriptional repressors, we have uncovered precise temporal control of their clearance by two distinct E3 ubiquitin ligase complexes: the SCF E3 ligase governs the degradation of SMG, whereas the CTLH E3 ligase is responsible for the degradation of Cup, TRAL, and ME31B. Intriguingly, SMG is degraded later during the MZT compared with its co-repressors Cup, TRAL, and ME31B. We have also shown that clearance of SMG is essential for appropriate levels of re-expression of a subset of its targets during ZGA. Our results raise questions about how temporal specificity of protein degradation is regulated, as well as why at least two temporally distinct mechanisms of protein degradation exist during the MZT.

Expression data support the hypothesis that timing of E3 ligase function might, at least in part, be determined by the timing of expression of one or more of their component subunits, notably Muskelin for CTLH and CG14317 for SCF. During the *Drosophila* MZT, most components of the CTLH complex display constant expression levels, but Muskelin protein is degraded with a similar profile to its target repressors. Mammalian Muskelin has been shown to be auto-ubiquitinated and targeted for degradation (Maitland et al., 2019). Our detection of a ubiquitinated peptide in Muskelin supports the possibility that the *Drosophila* CTLH complex may be negatively autoregulated through its Muskelin subunit during the MZT. In contrast, activation of CTLH function at the beginning of the MZT may not depend on changes in complex composition: previous studies have shown that going from stage 14 oocytes to activated eggs or early (0–1 h) embryos, there are no significant changes in either the levels of CTLH subunit proteins (including Muskelin) or the ribosome association of their cognate transcripts (Eichhorn et al., 2016; Kronja et al., 2014b). Thus, we speculate that post-translational modification of one or more CTLH subunits may activate CTLH function.

Modification of substrates may also play a role: the degradation of Cup, TRAL, and ME31B depends on the PNG kinase (Wang et al., 2017), which itself has temporally restricted activity coinciding with degradation of these repressors (Hara et al., 2017). PNG-dependent phosphorylation of Cup, TRAL, and ME31B may make them ubiquitination substrates. Furthermore, evidence suggests that temporal regulation of the E2

ubiquitin-conjugating enzyme, UBC-E2H, at this stage depends on the PNG kinase and may also contribute to the timing of ubiquitin ligase complex function during the MZT (Zavortink et al., 2019). Concomitant PNG-dependent activation of the CTLH complex, its cognate E2, and its substrates, coupled with subsequent self-inactivation of the complex through Muskelin degradation, would provide a precise time window for CTLH function and, therefore, for degradation of Cup, TRAL, and ME31B early in the MZT.

In contrast with these three co-repressors, degradation of SMG occurs near the end of the MZT and depends on zygotic gene expression. Although the levels of most SCF complex subunits are constant during the MZT, the F-box protein CG14317 displays a unique expression pattern: CG14317 protein and mRNA are absent at the beginning of the MZT, are zygotically synthesized, peak in NC14 embryos, and sharply decline shortly thereafter. Thus, CG14317 expression coincides with the timing of SMG protein degradation and, coupled with the zygotic nature of its accumulation, makes it a strong candidate to be a timer for SCF function. The fact that knockdown of SLMB stabilizes SMG protein suggests that both F-box proteins may be necessary for SMG degradation, with CG14317 serving as the timer. At present there are no forward or reverse genetic reagents available to test this hypothesis. Additionally, the function of SLMB in directing SMG-protein ubiquitination may itself be temporally restricted. Both *Drosophila* SLMB and its mammalian homolog are known to bind phosphorylated motifs (Frescas and Pagano, 2008; Jia et al., 2005). Phosphorylated residues have been detected in SMG in the embryo, including residues within its C terminus (Zhai et al., 2008); one of these, S967, resides close to a ubiquitinated lysine, K965 (Table S3). In summary, despite the stable expression of SLMB during the MZT, temporal regulation of phosphorylation of its target proteins, including SMG, through yet uncharacterized mechanisms, may also contribute to temporal control of SMG protein degradation.

Because Cup, TRAL, and ME31B are known to function as co-repressors in a complex with SMG (Götze et al., 2017; Jeske et al., 2011; Nelson et al., 2004), why are the timing of degradation of Cup-TRAL-ME31B and SMG differentially regulated? Although the SMG-Cup-TRAL-ME31B-mRNA complex has been characterized to be extremely stable *in vitro* (Jeske et al., 2011), it would be disrupted *in vivo* by the degradation of Cup, TRAL, and ME31B (or by the degradation of *nos* and other SMG-target mRNAs). SMG directs translational repression both through AGO1 and through Cup-TRAL-ME31B, as well as transcript degradation through recruitment of the CCR4-NOT deadenylase (Chen et al., 2014; Nelson et al., 2004; Pinder and Smibert, 2013; Semotok et al., 2005; Tadros et al., 2007; Zaessinger et al., 2006). CTLH-driven degradation of Cup, TRAL, and ME31B would abrogate SMG-Cup-TRAL-ME31B-dependent translational repression, but not AGO1-dependent repression, because AGO1 levels increase during the MZT (Luo et al., 2016). However, the relative contributions of AGO1 versus Cup-TRAL-ME31B to translational repression by SMG are unknown. That said, the CCR4-NOT deadenylase is present both during and after the MZT (Temme et al., 2004); thus, SMG-dependent transcript degradation would occur both before and after clearance of Cup, TRAL, and ME31B. 12% of SMG-associated transcripts are degraded, but not repressed, by SMG (Chen et al., 2014). Perhaps this subset is bound and degraded by SMG late in the MZT, after the drop in Cup, TRAL, and ME31B levels.

Another possible role for clearance of ME31B and TRAL derives from studies in budding yeast, where it has been shown that their orthologs, respectively, Dhh1p and Scd6p, have a potent inhibitory effect on "general" translation (Coller and Parker, 2005; Nissan et al., 2010; Rajyaguru et al., 2012). If this is also true in *Drosophila*, then degradation of ME31B and TRAL, which are present at exceedingly high concentrations in embryos (Götze et al., 2017), might also serve to permit high-level translation during the second phase of the MZT (Wang et al., 2017).

We previously showed that SMG has both direct and indirect roles in the MZT. SMG's direct role is to bind to a large number of maternal mRNA species and target them for repression and/or degradation (Chen et al., 2014; Tadros et al., 2007). Two indirect effects have been shown in *smg* mutants. First, if maternal transcripts fail to be degraded and/or repressed, ZGA fails or is significantly delayed, likely because mRNAs encoding transcriptional repressors persist (Benoit et al., 2009; Luo et al., 2016). Second, because zygotically synthesized microRNAs direct a second wave of maternal mRNA decay during the late MZT, in *smg* mutants, failure to produce those microRNAs results in failure to eliminate a second set of maternal transcripts late in the MZT (Benoit et al., 2009; Luo et al., 2016).

Here we have uncovered a role for rapid clearance of the SMG protein itself late in the MZT: to permit normal levels of zygotic re-expression of a subset of it targets. Notably, stabilized SMG (SMG767Δ999) rescues both clearance of its maternal targets and ZGA, excluding the possibility that lower-than-normal levels of re-expressed targets are a result of defective SMG function upon deletion of its C terminus. Indeed, in our control experiments, SMG's exclusively maternal targets actually dropped to lower levels than normal, likely because SMG767Δ999 continues to direct their decay beyond when SMG normally disappears from embryos. Furthermore, in our other control, strictly zygotic transcripts that lack SMG binding sites were expressed at higher levels in SMG767Δ999-rescued mutants than in full-length SMG-rescued mutants. This result is consistent with the hypothesis that clearance of transcriptional repressors by SMG permits ZGA (Benoit et al., 2009); persistent SMG would clear these repressors to lower levels than normal, hence resulting in higher zygotic expression. The higher-than-normal expression of zygotic transcripts that lack SMG binding sites makes the lower-than-normal levels of SMG's zygotically re-expressed target transcripts by SMG767Δ999 even more striking. Together, these data support a model in which the timing of both SMG synthesis and clearance are important for orderly progression of the MZT.

STAR★METHODS

Detailed methods are provided in the online version of this paper and include the following:

- KEY RESOURCES TABLE
- RESOURCE AVAILABILITY

SUPPLEMENTAL INFORMATION

Supplemental Information can be found online at https://doi.org/10.1016/j.celrep.2020.107783.

ACKNOWLEDGMENTS

We thank Olivia Rissland for communicating unpublished results prior to submission of a related manuscript; Angelo Karaiskakis and Hua Luo for technical assistance at the University of Toronto; Andrea Sinz for supporting the MS measurements at the University of Halle; Paul Schedl, Eric Wieschaus, and Trudi Schüpbach for helpful advice and suggestions, and Lillia Ryazanova for technical assistance at Princeton University; Michael Götze, Luz Irina Calderon Villalobos, and Michael Niemeyer for helpful discussions in Halle; and Thomas Hurd for a critical review of the manuscript in Toronto. Antibodies were kindly provided by Akira Nakamura (rabbit anti-Cup, TRAL, ME31B) and Gregory Rogers (guinea pig anti-SLMB). W.X.C. was supported in part by an Ontario Graduate Scholarship and University of Toronto Open Scholarships. This research was supported by the following funding agencies: Canadian Institutes of Health Research (grant PJT-159702 to H.D.L.), Natural Sciences and Engineering Research Council of Canada (H.D.L. and C.A.S.), Deutsche Forschungsgemeinschaft (grant WA 548/17-1 within SPP 1935 to E.W.), and National Institutes of Health (grants R35GM128813 to M.W. and T32GM007388 to E.Y.).

AUTHOR CONTRIBUTIONS

The project was designed by H.D.L. and E.W. The unfertilized egg time course, RNAi experiments, analyses of FLAG-SMG and FLAG-SMG767Δ999 time course westerns, and qRT-PCR experiments to assess mRNAs in FLAG-SMG and FLAG-SMG767Δ999 were carried out by W.X.C. under the supervision of H.D.L.; the RBP western time course, MG132 experiments, and GFP-Muskelin/CG3295 westerns were carried out by S.K. under the supervision of E.W.; TMTc+ MS was carried out by M.G. and E.Y. under the supervision of M.W.; FLAG-SMG IP-MS was carried out by W.X.C. and S.L. under the supervision of H.D.L. and S.A., respectively; GFP-Muskelin and GFP-SLMB IP-MS were carried out by S.K., C.R., and C.I. under the supervision of E.W.; F.P. generated the anti-eIF4E and anti-CG3295 antibodies under the supervision of E.W.; T.C.H.L. wrote the script to calculate SRE scores under the supervision of H.D.L.; N.U.S. constructed the transgenes to express FLAG-SMG and FLAG-SMG767Δ999 under the supervision of H.D.L.; and M.H.K.C. showed that FLAG-SMG767Δ999 persists under the supervision of C.A.S. W.X.C. wrote the first draft of the manuscript, which was revised by H.D.L. with major input from E.W. and M.W., as well as input from the other co-authors.

DECLARATION OF INTERESTS

The authors declare no competing interests.

Received: March 25, 2020
Revised: May 6, 2020
Accepted: May 28, 2020
Published: June 23, 2020

REFERENCES

Aanes, H., Collas, P., and Aleström, P. (2014). Transcriptome dynamics and diversity in the early zebrafish embryo. Brief. Funct. Genomics *13*, 95–105.

Aviv, T., Lin, Z., Lau, S., Rendl, L.M., Sicheri, F., and Smibert, C.A. (2003). The RNA-binding SAM domain of Smaug defines a new family of post-transcriptional regulators. Nat. Struct. Biol. *10*, 614–621.

Aviv, T., Lin, Z., Ben-Ari, G., Smibert, C.A., and Sicheri, F. (2006). Sequence-specific recognition of RNA hairpins by the SAM domain of Vts1p. Nat. Struct. Mol. Biol. *13*, 168–176.

Bailey, T.L., and Elkan, C. (1994). Fitting a mixture model by expectation maximization to discover motifs in biopolymers. Proc. Int. Conf. Intell. Syst. Mol. Biol. *2*, 28–36.

Baltz, A.G., Munschauer, M., Schwanhäusser, B., Vasile, A., Murakawa, Y., Schueler, M., Youngs, N., Penfold-Brown, D., Drew, K., Milek, M., et al. (2012). The mRNA-bound proteome and its global occupancy profile on protein-coding transcripts. Mol. Cell *46*, 674–690.

Bashirullah, A., Halsell, S.R., Cooperstock, R.L., Kloc, M., Karaiskakis, A., Fisher, W.W., Fu, W., Hamilton, J.K., Etkin, L.D., and Lipshitz, H.D. (1999). Joint action of two RNA degradation pathways controls the timing of maternal transcript elimination at the midblastula transition in *Drosophila melanogaster*. EMBO J. *18*, 2610–2620.

Becker, K., Bluhm, A., Casas-Vila, N., Dinges, N., Dejung, M., Sayols, S., Kreutz, C., Roignant, J.Y., Butter, F., and Legewie, S. (2018). Quantifying post-transcriptional regulation in the development of Drosophila melanogaster. Nat. Commun. *9*, 4970.

Benoit, B., He, C.H., Zhang, F., Votruba, S.M., Tadros, W., Westwood, J.T., Smibert, C.A., Lipshitz, H.D., and Theurkauf, W.E. (2009). An essential role for the RNA-binding protein Smaug during the Drosophila maternal-to-zygotic transition. Development *136*, 923–932.

Brown, J.B., Boley, N., Eisman, R., May, G.E., Stoiber, M.H., Duff, M.O., Booth, B.W., Wen, J., Park, S., Suzuki, A.M., et al. (2014). Diversity and dynamics of the Drosophila transcriptome. Nature *512*, 393–399.

Brownlee, C.W., Klebba, J.E., Buster, D.W., and Rogers, G.C. (2011). The Protein Phosphatase 2A regulatory subunit Twins stabilizes Plk4 to induce centriole amplification. J. Cell Biol. *195*, 231–243.

Casas-Vila, N., Bluhm, A., Sayols, S., Dinges, N., Dejung, M., Altenhein, T., Kappei, D., Altenhein, B., Roignant, J.Y., and Butter, F. (2017). The developmental proteome of *Drosophila melanogaster*. Genome Res. *27*, 1273–1285.

Chartier, A., Klein, P., Pierson, S., Barbezier, N., Gidaro, T., Casas, F., Carberry, S., Dowling, P., Maynadier, L., Bellec, M., et al. (2015). Mitochondrial dysfunction reveals the role of mRNA poly(A) tail regulation in oculopharyngeal muscular dystrophy pathogenesis. PLoS Genet. *11*, e1005092.

Chen, L., Dumelie, J.G., Li, X., Cheng, M.H., Yang, Z., Laver, J.D., Siddiqui, N.U., Westwood, J.T., Morris, Q., Lipshitz, H.D., and Smibert, C.A. (2014). Global regulation of mRNA translation and stability in the early Drosophila embryo by the Smaug RNA-binding protein. Genome Biol. *15*, R4.

Chiu, C.W.N., Monat, C., Robitaille, M., Lacomme, M., Daulat, A.M., Macleod, G., McNeill, H., Cayouette, M., and Angers, S. (2016). SAPCD2 controls spindle orientation and asymmetric divisions by negatively regulating the Gαi-LGN-NuMA ternary complex. Dev. Cell *36*, 50–62.

Choi, H., Larsen, B., Lin, Z.Y., Breitkreutz, A., Mellacheruvu, D., Fermin, D., Qin, Z.S., Tyers, M., Gingras, A.C., and Nesvizhskii, A.I. (2011). SAINT: probabilistic scoring of affinity purification-mass spectrometry data. Nat. Methods *8*, 70–73.

Coller, J., and Parker, R. (2005). General translational repression by activators of mRNA decapping. Cell *122*, 875–886.

Cox, J., and Mann, M. (2008). MaxQuant enables high peptide identification rates, individualized p.p.b.-range mass accuracies and proteome-wide protein quantification. Nat. Biotechnol. *26*, 1367–1372.

Dahanukar, A., Walker, J.A., and Wharton, R.P. (1999). Smaug, a novel RNA-binding protein that operates a translational switch in Drosophila. Mol. Cell *4*, 209–218.

De Renzis, S., Elemento, O., Tavazoie, S., and Wieschaus, E.F. (2007). Unmasking activation of the zygotic genome using chromosomal deletions in the Drosophila embryo. PLoS Biol. *5*, e117.

Du, Z., He, F., Yu, Z., Bowerman, B., and Bao, Z. (2015). E3 ubiquitin ligases promote progression of differentiation during C. elegans embryogenesis. Dev. Biol. *398*, 267–279.

Edgar, B.A., Sprenger, F., Duronio, R.J., Leopold, P., and O'Farrell, P.H. (1994). Distinct molecular mechanism regulate cell cycle timing at successive stages of Drosophila embryogenesis. Genes Dev. *8*, 440–452.

Eichhorn, S.W., Subtelny, A.O., Kronja, I., Kwasnieski, J.C., Orr-Weaver, T.L., and Bartel, D.P. (2016). mRNA poly(A)-tail changes specified by deadenylation broadly reshape translation in Drosophila oocytes and early embryos. eLife *5*, e16955.

Elfring, L.K., Axton, J.M., Fenger, D.D., Page, A.W., Carminati, J.L., and Orr-Weaver, T.L. (1997). Drosophila PLUTONIUM protein is a specialized cell cycle regulator required at the onset of embryogenesis. Mol. Biol. Cell *8*, 583–593.

Elias, J.E., and Gygi, S.P. (2007). Target-decoy search strategy for increased confidence in large-scale protein identifications by mass spectrometry. Nat. Methods *4*, 207–214.

Fabre, B., Korona, D., Groen, A., Vowinckel, J., Gatto, L., Deery, M.J., Ralser, M., Russell, S., and Lilley, K.S. (2016). Analysis of Drosophila melanogaster proteome dynamics during embryonic development by a combination of label-free proteomics approaches. Proteomics *16*, 2068–2080.

Farrell, J.A., and O'Farrell, P.H. (2013). Mechanism and regulation of Cdc25/Twine protein destruction in embryonic cell-cycle remodeling. Curr. Biol. *23*, 118–126.

Fenger, D.D., Carminati, J.L., Burney-Sigman, D.L., Kashevsky, H., Dines, J.L., Elfring, L.K., and Orr-Weaver, T.L. (2000). PAN GU: a protein kinase that inhibits S phase and promotes mitosis in early Drosophila development. Development *127*, 4763–4774.

Francis, O., Han, F., and Adams, J.C. (2013). Molecular phylogeny of a RING E3 ubiquitin ligase, conserved in eukaryotic cells and dominated by homologous components, the muskelin/RanBPM/CTLH complex. PLoS ONE *8*, e75217.

Frescas, D., and Pagano, M. (2008). Deregulated proteolysis by the F-box proteins SKP2 and beta-TrCP: tipping the scales of cancer. Nat. Rev. Cancer *8*, 438–449.

Götze, M., Dufourt, J., Ihling, C., Rammelt, C., Pierson, S., Sambrani, N., Temme, C., Sinz, A., Simonelig, M., and Wahle, E. (2017). Translational repression of the *Drosophila nanos* mRNA involves the RNA helicase Belle and RNA coating by Me31B and Trailer hitch. RNA *23*, 1552–1568.

Gouw, J.W., Pinkse, M.W., Vos, H.R., Moshkin, Y., Verrijzer, C.P., Heck, A.J., and Krijgsveld, J. (2009). In vivo stable isotope labeling of fruit flies reveals post-transcriptional regulation in the maternal-to-zygotic transition. Mol. Cell. Proteomics *8*, 1566–1578.

Graveley, B.R., Brooks, A.N., Carlson, J.W., Duff, M.O., Landolin, J.M., Yang, L., Artieri, C.G., van Baren, M.J., Boley, N., Booth, B.W., et al. (2011). The developmental transcriptome of Drosophila melanogaster. Nature *471*, 473–479.

Groth, A.C., Fish, M., Nusse, R., and Calos, M.P. (2004). Construction of transgenic Drosophila by using the site-specific integrase from phage phiC31. Genetics *166*, 1775–1782.

Gupta, M., Sonnett, M., Ryazanova, L., Presler, M., and Wühr, M. (2018). Quantitative proteomics of Xenopus embryos I, sample preparation. Methods Mol. Biol. *1865*, 175–194.

Guven-Ozkan, T., Nishi, Y., Robertson, S.M., and Lin, R. (2008). Global transcriptional repression in C. elegans germline precursors by regulated sequestration of TAF-4. Cell *135*, 149–160.

Hara, M., Petrova, B., and Orr-Weaver, T.L. (2017). Control of PNG kinase, a key regulator of mRNA translation, is coupled to meiosis completion at egg activation. eLife *6*, e22219.

Hara, M., Lourido, S., Petrova, B., Lou, H.J., Von Stetina, J.R., Kashevsky, H., Turk, B.E., and Orr-Weaver, T.L. (2018). Identification of PNG kinase substrates uncovers interactions with the translational repressor TRAL in the oocyte-to-embryo transition. eLife *7*, e33150.

Harnisch, C., Cuzic-Feltens, S., Dohm, J.C., Götze, M., Himmelbauer, H., and Wahle, E. (2016). Oligoadenylation of 3′ decay intermediates promotes cytoplasmic mRNA degradation in Drosophila cells. RNA *22*, 428–442.

Higuchi, C., Shimizu, N., Shin, S.W., Morita, K., Nagai, K., Anzai, M., Kato, H., Mitani, T., Yamagata, K., Hosoi, Y., et al. (2018). Ubiquitin-proteasome system modulates zygotic genome activation in early mouse embryos and influences full-term development. J. Reprod. Dev. *64*, 65–74.

Ho, M.S., Tsai, P.I., and Chien, C.T. (2006). F-box proteins: the key to protein degradation. J. Biomed. Sci. *13*, 181–191.

Huang, W., Sherman, B.T., and Lempicki, R.A. (2009a). Bioinformatics enrichment tools: paths toward the comprehensive functional analysis of large gene lists. Nucleic Acids Res. *37*, 1–13.

Huang, D.W., Sherman, B.T., Zheng, X., Yang, J., Imamichi, T., Stephens, R., and Lempicki, R.A. (2009b). Extracting biological meaning from large gene lists with DAVID. Curr. Protoc. Bioinformatics *27*, 13.11.1–13.11.13.

Huttlin, E.L., Jedrychowski, M.P., Elias, J.E., Goswami, T., Rad, R., Beausoleil, S.A., Villén, J., Haas, W., Sowa, M.E., and Gygi, S.P. (2010). A tissue-specific atlas of mouse protein phosphorylation and expression. Cell *143*, 1174–1189.

Jeske, M., Moritz, B., Anders, A., and Wahle, E. (2011). Smaug assembles an ATP-dependent stable complex repressing nanos mRNA translation at multiple levels. EMBO J. *30*, 90–103.

Jia, J., Zhang, L., Zhang, Q., Tong, C., Wang, B., Hou, F., Amanai, K., and Jiang, J. (2005). Phosphorylation by double-time/CKIepsilon and CKIalpha targets cubitus interruptus for Slimb/beta-TRCP-mediated proteolytic processing. Dev. Cell *9*, 819–830.

Jiang, T., McKinley, R.F., McGill, M.A., Angers, S., and Harris, T.J. (2015). A Par-1-Par-3-centrosome cell polarity pathway and its tuning for isotropic cell adhesion. Curr. Biol. *25*, 2701–2708.

Kisielnicka, E., Minasaki, R., and Eckmann, C.R. (2018). MAPK signaling couples SCF-mediated degradation of translational regulators to oocyte meiotic progression. Proc. Natl. Acad. Sci. USA *115*, E2772–E2781.

Komander, D., and Rape, M. (2012). The ubiquitin code. Annu. Rev. Biochem. *81*, 203–229.

Kronja, I., Whitfield, Z.J., Yuan, B., Dzeyk, K., Kirkpatrick, J., Krijgsveld, J., and Orr-Weaver, T.L. (2014a). Quantitative proteomics reveals the dynamics of protein changes during Drosophila oocyte maturation and the oocyte-to-embryo transition. Proc. Natl. Acad. Sci. USA *111*, 16023–16028.

Kronja, I., Yuan, B., Eichhorn, S.W., Dzeyk, K., Krijgsveld, J., Bartel, D.P., and Orr-Weaver, T.L. (2014b). Widespread changes in the posttranscriptional landscape at the Drosophila oocyte-to-embryo transition. Cell Rep. *7*, 1495–1508.

Lange, S.J., Maticzka, D., Möhl, M., Gagnon, J.N., Brown, C.M., and Backofen, R. (2012). Global or local? Predicting secondary structure and accessibility in mRNAs. Nucleic Acids Res. *40*, 5215–5226.

Laver, J.D., Li, X., Ray, D., Cook, K.B., Hahn, N.A., Nabeel-Shah, S., Kekis, M., Luo, H., Marsolais, A.J., Fung, K.Y., et al. (2015). Brain tumor is a sequence-specific RNA-binding protein that directs maternal mRNA clearance during the Drosophila maternal-to-zygotic transition. Genome Biol. *16*, 94.

Liu, H., and Pfirrmann, T. (2019). The Gid-complex: an emerging player in the ubiquitin ligase league. Biol. Chem. *400*, 1429–1441.

Liu, G., Zhang, J., Larsen, B., Stark, C., Breitkreutz, A., Lin, Z.Y., Breitkreutz, B.J., Ding, Y., Colwill, K., Pasculescu, A., et al. (2010). ProHits: integrated software for mass spectrometry-based interaction proteomics. Nat. Biotechnol. *28*, 1015–1017.

Liu, Y.C., Couzens, A.L., Deshwar, A.R., McBroom-Cerajewski, L.D., Zhang, X., Puviindran, V., Scott, I.C., Gingras, A.-C., Hui, C.-C., and Angers, S. (2014). The PPFIA1-PP2A protein complex promotes trafficking of Kif7 to the ciliary tip and Hedgehog signaling. Sci. Signal. *7*, ra117.

Lorenz, R., Bernhart, S.H., Höner Zu Siederdissen, C., Tafer, H., Flamm, C., Stadler, P.F., and Hofacker, I.L. (2011). ViennaRNA Package 2.0. Algorithms Mol. Biol. *6*, 26.

Luo, H., Li, X., Claycomb, J.M., and Lipshitz, H.D. (2016). The Smaug RNA-binding protein is essential for microRNA synthesis during the *Drosophila* maternal-to-zygotic transition. G3 (Bethesda) *6*, 3541–3551.

Maitland, M.E.R., Onea, G., Chiasson, C.A., Wang, X., Ma, J., Moor, S.E., Barber, K.R., Lajoie, G.A., Shaw, G.S., and Schild-Poulter, C. (2019). The mammalian CTLH complex is an E3 ubiquitin ligase that targets its subunit muskelin for degradation. Sci. Rep. *9*, 9864.

Markstein, M., Pitsouli, C., Villalta, C., Celniker, S.E., and Perrimon, N. (2008). Exploiting position effects and the gypsy retrovirus insulator to engineer precisely expressed transgenes. Nat. Genet. *40*, 476–483.

Matthews, B.B., Dos Santos, G., Crosby, M.A., Emmert, D.B., St Pierre, S.E., Gramates, L.S., Zhou, P., Schroeder, A.J., Falls, K., Strelets, V., et al.; FlyBase Consortium (2015). Gene Model Annotations for Drosophila melanogaster: Impact of High-Throughput Data. G3 (Bethesda) *5*, 1721–1736.

Mirali, S., Botham, A., Voisin, V., Xu, C., St-Germain, J., Sharon, D., Hoff, F.W., Qiu, Y., Hurren, R., Gronda, M., et al. (2020). The mitochondrial peptidase, neurolysin, regulates respiratory chain supercomplex formation and is necessary for AML viability. Sci. Transl. Med. *12*, eaaz8264.

Morais-de-Sá, E., Vega-Rioja, A., Trovisco, V., and St Johnston, D. (2013). Oskar is targeted for degradation by the sequential action of Par-1, GSK-3, and the SCF^{-}Slimb ubiquitin ligase. Dev. Cell *26*, 303–314.

Nakamura, A., Amikura, R., Hanyu, K., and Kobayashi, S. (2001). Me31B silences translation of oocyte-localizing RNAs through the formation of cytoplasmic RNP complex during Drosophila oogenesis. Development *128*, 3233–3242.

Nakamura, A., Sato, K., and Hanyu-Nakamura, K. (2004). Drosophila cup is an eIF4E binding protein that associates with Bruno and regulates oskar mRNA translation in oogenesis. Dev. Cell *6*, 69–78.

Nelson, M.R., Leidal, A.M., and Smibert, C.A. (2004). Drosophila Cup is an eIF4E-binding protein that functions in Smaug-mediated translational repression. EMBO J. *23*, 150–159.

Nissan, T., Rajyaguru, P., She, M., Song, H., and Parker, R. (2010). Decapping activators in Saccharomyces cerevisiae act by multiple mechanisms. Mol. Cell *39*, 773–783.

Noureddine, M.A., Donaldson, T.D., Thacker, S.A., and Duronio, R.J. (2002). Drosophila Roc1a encodes a RING-H2 protein with a unique function in processing the Hh signal transducer Ci by the SCF E3 ubiquitin ligase. Dev. Cell *2*, 757–770.

Page, A.W., and Orr-Weaver, T.L. (1997). Activation of the meiotic divisions in Drosophila oocytes. Dev. Biol. *183*, 195–207.

Pappireddi, N., Martin, L., and Wühr, M. (2019). A review on quantitative multiplexed proteomics. ChemBioChem *20*, 1210–1224.

Pérez-Montero, S., Carbonell, A., Morán, T., Vaquero, A., and Azorín, F. (2013). The embryonic linker histone H1 variant of Drosophila, dBigH1, regulates zygotic genome activation. Dev. Cell *26*, 578–590.

Peshkin, L., Gupta, M., Ryazanova, L., and Wühr, M. (2019). Bayesian confidence intervals for multiplexed proteomics integrate ion-statistics with peptide quantification concordance. Mol. Cell. Proteomics *18*, 2108–2120.

Peshkin, L., Wühr, M., Pearl, E., Haas, W., Freeman, R.M., Jr., Gerhart, J.C., Klein, A.M., Horb, M., Gygi, S.P., and Kirschner, M.W. (2015). On the relationship of protein and mRNA dynamics in vertebrate embryonic development. Dev. Cell *35*, 383–394.

Pickart, C.M. (2001). Mechanisms underlying ubiquitination. Annu. Rev. Biochem. *70*, 503–533.

Pinder, B.D., and Smibert, C.A. (2013). microRNA-independent recruitment of Argonaute 1 to nanos mRNA through the Smaug RNA-binding protein. EMBO Rep. *14*, 80–86.

Rajyaguru, P., She, M., and Parker, R. (2012). Scd6 targets eIF4G to repress translation: RGG motif proteins as a class of eIF4G-binding proteins. Mol. Cell *45*, 244–254.

Rand, M.D., Kearney, A.L., Dao, J., and Clason, T. (2010). Permeabilization of Drosophila embryos for introduction of small molecules. Insect Biochem. Mol. Biol. *40*, 792–804.

Ravid, T., and Hochstrasser, M. (2008). Diversity of degradation signals in the ubiquitin-proteasome system. Nat. Rev. Mol. Cell Biol. *9*, 679–690.

Rissland, O.S., Subtelny, A.O., Wang, M., Lugowski, A., Nicholson, B., Laver, J.D., Sidhu, S.S., Smibert, C.A., Lipshitz, H.D., and Bartel, D.P. (2017). The influence of microRNAs and poly(A) tail length on endogenous mRNA-protein complexes. Genome Biol. *18*, 211.

Savitski, M.M., Wilhelm, M., Hahne, H., Kuster, B., and Bantscheff, M. (2015). A scalable approach for protein false discovery rate estimation in large proteomic data sets. Mol. Cell. Proteomics *14*, 2394–2404.

Schneider, C.A., Rasband, W.S., and Eliceiri, K.W. (2012). NIH Image to ImageJ: 25 years of image analysis. Nat. Methods *9*, 671–675.

Semotok, J.L., Cooperstock, R.L., Pinder, B.D., Vari, H.K., Lipshitz, H.D., and Smibert, C.A. (2005). Smaug recruits the CCR4/POP2/NOT deadenylase complex to trigger maternal transcript localization in the early Drosophila embryo. Curr. Biol. *15*, 284–294.

Semotok, J.L., Luo, H., Cooperstock, R.L., Karaiskakis, A., Vari, H.K., Smibert, C.A., and Lipshitz, H.D. (2008). Drosophila maternal Hsp83 mRNA destabilization is directed by multiple SMAUG recognition elements in the open reading frame. Mol. Cell. Biol. *28*, 6757–6772.

Shirayama, M., Soto, M.C., Ishidate, T., Kim, S., Nakamura, K., Bei, Y., van den Heuvel, S., and Mello, C.C. (2006). The conserved kinases CDK-1, GSK-3, KIN-19, and MBK-2 promote OMA-1 destruction to regulate the oocyte-to-embryo transition in C. elegans. Curr. Biol. *16*, 47–55.

Shteynberg, D., Deutsch, E.W., Lam, H., Eng, J.K., Sun, Z., Tasman, N., Mendoza, L., Moritz, R.L., Aebersold, R., and Nesvizhskii, A.I. (2011). iProphet: multi-level integrative analysis of shotgun proteomic data improves peptide and protein identification rates and error estimates. Mol. Cell Proteomics *10*, M111.007690.

Siddiqui, N.U., Li, X., Luo, H., Karaiskakis, A., Hou, H., Kislinger, T., Westwood, J.T., Morris, Q., and Lipshitz, H.D. (2012). Genome-wide analysis of the maternal-to-zygotic transition in Drosophila primordial germ cells. Genome Biol. *13*, R11.

Sonnett, M., Gupta, M., Nguyen, T., and Wühr, M. (2018). Quantitative proteomics for Xenopus embryos II, data analysis. Methods Mol. Biol. *1865*, 195–215.

Sonnett, M., Yeung, E., and Wühr, M. (2018). Accurate, sensitive, and precise multiplexed proteomics using the complement reporter ion cluster. Anal. Chem. *90*, 5032–5039.

Stoeckius, M., Grün, D., Kirchner, M., Ayoub, S., Torti, F., Piano, F., Herzog, M., Selbach, M., and Rajewsky, N. (2014). Global characterization of the

oocyte-to-embryo transition in Caenorhabditis elegans uncovers a novel mRNA clearance mechanism. EMBO J. *33*, 1751–1766.

Strecker, T.R., McGhee, S., Shih, S., and Ham, D. (1994). Permeabilization, staining and culture of living Drosophila embryos. Biotech. Histochem. *69*, 25–30.

Subtelny, A.O., Eichhorn, S.W., Chen, G.R., Sive, H., and Bartel, D.P. (2014). Poly(A)-tail profiling reveals an embryonic switch in translational control. Nature *508*, 66–71.

Svoboda, P., Franke, V., and Schultz, R.M. (2015). Sculpting the transcriptome during the oocyte-to-embryo transition in mouse. Curr. Top. Dev. Biol. *113*, 305–349.

Sysoev, V.O., Fischer, B., Frese, C.K., Gupta, I., Krijgsveld, J., Hentze, M.W., Castello, A., and Ephrussi, A. (2016). Global changes of the RNA-bound proteome during the maternal-to-zygotic transition in Drosophila. Nat. Commun. *7*, 12128.

Tadros, W., and Lipshitz, H.D. (2009). The maternal-to-zygotic transition: a play in two acts. Development *136*, 3033–3042.

Tadros, W., Houston, S.A., Bashirullah, A., Cooperstock, R.L., Semotok, J.L., Reed, B.H., and Lipshitz, H.D. (2003). Regulation of maternal transcript destabilization during egg activation in Drosophila. Genetics *164*, 989–1001.

Tadros, W., Goldman, A.L., Babak, T., Menzies, F., Vardy, L., Orr-Weaver, T., Hughes, T.R., Westwood, J.T., Smibert, C.A., and Lipshitz, H.D. (2007). SMAUG is a major regulator of maternal mRNA destabilization in Drosophila and its translation is activated by the PAN GU kinase. Dev. Cell *12*, 143–155.

Tang, X., Orlicky, S., Lin, Z., Willems, A., Neculai, D., Ceccarelli, D., Mercurio, F., Shilton, B.H., Sicheri, F., and Tyers, M. (2007). Suprafacial orientation of the SCFCdc4 dimer accommodates multiple geometries for substrate ubiquitination. Cell *129*, 1165–1176.

Temme, C., Zaessinger, S., Meyer, S., Simonelig, M., and Wahle, E. (2004). A complex containing the CCR4 and CAF1 proteins is involved in mRNA deadenylation in Drosophila. EMBO J. *23*, 2862–2871.

Thomsen, S., Anders, S., Janga, S.C., Huber, W., and Alonso, C.R. (2010). Genome-wide analysis of mRNA decay patterns during early Drosophila development. Genome Biol. *11*, R93.

Ting, L., Rad, R., Gygi, S.P., and Haas, W. (2011). MS3 eliminates ratio distortion in isobaric multiplexed quantitative proteomics. Nat. Methods *8*, 937–940.

Tsukamoto, T., Gearhart, M.D., Spike, C.A., Huelgas-Morales, G., Mews, M., Boag, P.R., Beilharz, T.H., and Greenstein, D. (2017). LIN-41 and OMA ribonucleoprotein complexes mediate a translational repression-to-activation switch controlling oocyte meiotic maturation and the oocyte-to-embryo transition in *Caenorhabditis elegans*. Genetics *206*, 2007–2039.

Vardy, L., and Orr-Weaver, T.L. (2007). The Drosophila PNG kinase complex regulates the translation of cyclin B. Dev. Cell *12*, 157–166.

Vastenhouw, N.L., Cao, W.X., and Lipshitz, H.D. (2019). The maternal-to-zygotic transition revisited. Development *146*, dev161471.

Wang, C., Uversky, V.N., and Kurgan, L. (2016). Disordered nucleiome: Abundance of intrinsic disorder in the DNA- and RNA-binding proteins in 1121 species from Eukaryota, Bacteria and Archaea. Proteomics *16*, 1486–1498.

Wang, M., Ly, M., Lugowski, A., Laver, J.D., Lipshitz, H.D., Smibert, C.A., and Rissland, O.S. (2017). ME31B globally represses maternal mRNAs by two distinct mechanisms during the *Drosophila* maternal-to-zygotic transition. eLife *6*, e27891.

Wilhelm, J.E., Mansfield, J., Hom-Booher, N., Wang, S., Turck, C.W., Hazelrigg, T., and Vale, R.D. (2000). Isolation of a ribonucleoprotein complex involved in mRNA localization in Drosophila oocytes. J. Cell Biol. *148*, 427–440.

Wilhelm, J.E., Hilton, M., Amos, Q., and Henzel, W.J. (2003). Cup is an eIF4E binding protein required for both the translational repression of oskar and the recruitment of Barentsz. J. Cell Biol. *163*, 1197–1204.

Winata, C.L., Łapiński, M., Pryszcz, L., Vaz, C., Bin Ismail, M.H., Nama, S., Hajan, H.S., Lee, S.G.P., Korzh, V., Sampath, P., et al. (2018). Cytoplasmic polyadenylation-mediated translational control of maternal mRNAs directs maternal-to-zygotic transition. Development *145*, dev159566.

Wojcik, E.J., Glover, D.M., and Hays, T.S. (2000). The SCF ubiquitin ligase protein slimb regulates centrosome duplication in Drosophila. Curr. Biol. *10*, 1131–1134.

Wühr, M., Freeman, R.M., Jr., Presler, M., Horb, M.E., Peshkin, L., Gygi, S., and Kirschner, M.W. (2014). Deep proteomics of the Xenopus laevis egg using an mRNA-derived reference database. Curr. Biol. *24*, 1467–1475.

Yang, Y., Zhou, C., Wang, Y., Liu, W., Liu, C., Wang, L., Liu, Y., Shang, Y., Li, M., Zhou, S., et al. (2017). The E3 ubiquitin ligase RNF114 and TAB1 degradation are required for maternal-to-zygotic transition. EMBO Rep. *18*, 205–216.

Zaessinger, S., Busseau, I., and Simonelig, M. (2006). Oskar allows nanos mRNA translation in Drosophila embryos by preventing its deadenylation by Smaug/CCR4. Development *133*, 4573–4583.

Zavortink, M., Rutt, L.N., Dzitoyeva, S., Barrington, C., Bilodeau, D.Y., Wang, M., Chen, X.X.L., and Rissland, O.S. (2019). Egg activation triggers clearance of maternally deposited RNA binding proteins. bioRxiv. https://doi.org/10.1101/806968.

Zhai, B., Villén, J., Beausoleil, S.A., Mintseris, J., and Gygi, S.P. (2008). Phosphoproteome analysis of Drosophila melanogaster embryos. J. Proteome Res. *7*, 1675–1682.

Zheng, N., and Shabek, N. (2017). Ubiquitin ligases: structure, function, and regulation. Annu. Rev. Biochem. *86*, 129–157.

STAR★METHODS

KEY RESOURCES TABLE

REAGENT or RESOURCE	SOURCE	IDENTIFIER
Antibodies		
α-Cup rat polyclonal	Akira Nakamura	Nakamura et al., 2004; RRID: AB_2568985
α-ME31B rabbit polyclonal	Akira Nakamura	Nakamura et al., 2001; RRID: AB_2568986
α-ME31B rabbit polyclonal	Elmar Wahle	Harnisch et al., 2016
α-TRAL rabbit polyclonal	Akira Nakamura	Nakamura et al., 2001
α-TRAL rat polyclonal	Elmar Wahle	Götze et al., 2017
α-SMG guinea pig polyclonal	Craig Smibert	Tadros et al., 2007
α-SMG rabbit polyclonal	Elmar Wahle	Chartier et al., 2015; RRID: AB_2567238
α-BEL rabbit polyclonal	Elmar Wahle	Götze et al., 2017
α-SLMB guinea pig polyclonal	Gregory Rogers	Brownlee et al., 2011; RRID: AB_2567136
α-eIF4E rat polyclonal	This paper	N/A
α-CG3295 rat polyclonal	This paper	N/A
α-alpha-Tubulin mouse monoclonal	Sigma-Aldrich	Cat#T5168; RRID: AB_477579
α-Actin mouse monoclonal	Sigma-Aldrich	Cat#A4700; RRID: AB_476730
Cy3 AffiniPure Donkey α-guinea pig IgG (H+L)	Jackson ImmunoResearch	Cat#706-165-148; RRID: AB_2340460
Peroxidase AffiniPure Goat Anti-Guinea Pig IgG (H+L)	Jackson ImmunoResearch	Cat#106-035-003; RRID: AB_2337402
Peroxidase AffiniPure Goat Anti-Rat IgG (H+L)	Jackson ImmunoResearch	Cat# 112-035-003; RRID: AB_2338128
Peroxidase AffiniPure Goat Anti-Mouse IgG (H+L)	Jackson ImmunoResearch	Cat#115-035-003; RRID: AB_10015289
Peroxidase AffiniPure Goat Anti-Rabbit IgG (H+L)	Jackson ImmunoResearch	Cat#111-035-114; RRID: AB_2307391
IRDye800CW Donkey Anti-Rabbit IgG	LI-COR	Cat#926-32211; RRID: AB_621843
IRDye800CW Goat Anti-Rat IgG	LI-COR	Cat#926-32219; RRID: AB_1850025
IRDye680 Donkey Anti-Mouse IgG	Li-COR	Cat#926-32222; RRID: AB_621844
α-FLAG M2 Affinity Gel	Sigma-Aldrich	Cat#A2220; RRID: AB_10063035
Protein A-Agarose	Roche	Cat#11134515001
Protein A-Sepharose CL-4B	GE Healthcare	Cat#17-0780-01
GFP-Trap Agarose	Chromotek	Cat#gta-20; RRID: AB_2631357
Chemicals, Peptides, and Recombinant Proteins		
Pierce Protease Inhibitor Tablets	Thermo Scientific	Cat#PI88666
Lysyl Endopeptidase (Lys-C)	Wako Pure Chemical	Cat#125-05061
Sequencing Grade Modified Trypsin	Promega	Cat#V5111
MG-132	Biomol GmbH	Cat#AG-CP3-0011-M005
(R)-(+)-limonene	Merck	Cat#8.18407.0500
PR 619, DUB inhibitor	Abcam	Cat#ab144641
AEBSF	Bioshop	Cat#AEB602
Benzamidine	Bioshop	Cat#BEN666
Pepstatin	Bioshop	Cat#PEP605
Leupeptin	Bioshop	Cat#LEU001
RNase A	Thermo Scientific	Cat#EN0531
Pierce Trypsin Protease, MS Grade	Thermo Scientific	Cat#90305
TRI Reagent	Sigma-Aldrich	Cat#93289

(*Continued on next page*)

Continued

REAGENT or RESOURCE	SOURCE	IDENTIFIER
DAPI	Sigma-Aldrich	Cat#D9542
DABCO	Sigma-Aldrich	Cat#D27802
Critical Commercial Assays		
Immobilon Crescendo Western HRP substrate	Millipore	Cat#WLBUR0100
Quick Start Bradford Protein Assay	Bio-Rad	Cat#5000201
SuperScript IV First-Strand Synthesis System	Invitrogen	Cat#18091050
SensiFAST SYBR No-Rox Kit	Bioline	Cat#BIO-98050
TMT labeling reagents	ThermoFisher	Cat#90062
Pierce PCA Protein Assay Kit	Thermo Scientific	Cat#23225
C18 Sep-Pak	Water Corporations	Cat#WAT054955
Pierce C18 Spin Tips	Thermo Scientific	Cat#84850
Deposited Data		
embryo developmental proteome raw data	This paper	ProteomeXchange: PXD016523
FLAG-SMG IP-MS raw data	This paper	ProteomeXchange: PXD019280
GFP-SLMB and Muskelin-GFP IP-MS raw data	This paper	ProteomeXchange: PXD018794
Drosophila embryo developmental proteome	Casas-Vila et al., 2017	N/A
Drosophila embryo mRNA abundance and mRNA translation efficiency	Eichhorn et al., 2016	N/A
Flybase Transcriptome release 6.13 (Sept 2016)	FlyBase Consortium	ftp://ftp.flybase.net/genomes/Drosophila_melanogaster/dmel_r6.13_FB2016_05/fasta/
Experimental Models: Organisms/Strains		
D. melanogaster: w^{1118}	Bloomington Drosophila Stock Center (BDSC)	Stock #3605
D. melanogaster: Canton S	G. Reuter, University of Halle	BDSC # 64349
D. melanogaster: P{UAS:GFP-slmb-6}/CyO	Daniel St Johnston	Morais-de-Sá et al., 2013
D. melanogaster: w; P{UAS-muskelin.GFP} attP2*	BDSC	Stock #65860
D. melanogaster: w^{1118}; P{GAL4::VP16-nos.UTR}CG6325^{MVD1}	BDSC	Stock #4937
D. melanogaster: muskelin RNAi: *y[1] v[1]; P{y[+t7.7] v[+t1.8] = TRiP.GLC01768}attP40*	BDSC	Stock #51405
D. melanogaster: ranBPM RNAi: *y[1] sc[*] v[1] sev[21]; P{y[+t7.7]v[+t1.8] = TRiP.HMC05142}attP40*	BDSC	Stock #61172
D. melanogaster: CG3295 RNAi: *y[1] v[1]; P{y[+t7.7] v[+t1.8] = TRiP.HMJ23451}attP40*	BDSC	Stock #61896
D. melanogaster: cul1 RNAi: *y[1] sc[*] v[1] sev[21]; P{y[+t7.7] v[+t1.8] = TRiP.GL00561} attP2*	BDSC	Stock #36601
D. melanogaster: skpA RNAi: *y[1] sc[*] v[1] sev[21]; P{y[+t7.7] v[+t1.8] = TRiP.HMS00791}attP2*	BDSC	Stock #32991
D. melanogaster: slmb RNAi: *y[1] sc[*] v[1] sev[21]; P{y[+t7.7] v[+t1.8] = TRiP.HMS00838}attP2*	BDSC	Stock #33898

(*Continued on next page*)

Continued

REAGENT or RESOURCE	SOURCE	IDENTIFIER
D. melanogaster: mCherry RNAi: *y[1] sc[*] v [1] sev[21]; P{y[+t7.7] v[+t1.8] = VALIUM20-mCherry}attP2*	Thomas Hurd, University of Toronto	BDSC #35785
D. melanogaster: y[1] w[*]; P{matalpha4-GAL-VP16}67; P{matalpha4-GAL-VP16}15	BDSC	Stock #80361
D. melanogaster: w; smg^{47}/Tm3*	Craig Smibert	Chen et al., 2014
D. melanogaster: w; P{w[+mC] = FLAG-smg}attp40; smg^{47}*	This paper	N/A
D. melanogaster: w P{w[+mC] = FLAG-smg767Δ999}attp40; smg^{47}*	This paper	N/A
Oligonucleotides		
Random Hexamer Primer	Thermo Scientific	Cat#SO142
Primers used for qPCR experiments: see Table S6	This paper	N/A
Software and Algorithms		
kmeans clustering	MATLAB kmeans	MATLAB 2019a
BACIQ	Peshkin et al., 2019	https://github.com/wuhrlab/BACIQ
GFY software	Huttlin et al., 2010	https://gygi.med.harvard.edu/
DAVID 6.8 functional annotation tool web server	Huang et al., 2009b	https://david.ncifcrf.gov/
MEME Multiple Em for Motif Elicitation	Bailey and Elkan, 1994	http://meme-suite.org/tools/meme
ProHits Software Package	Liu et al., 2010	http://prohitsms.com/Prohits_download/list.php
MaxQuant 1.6.1.0	Cox and Mann, 2008	https://maxquant.org
Image Lab 6.0	Bio-Rad	N/A
Image Studio Lite	LI-COR	N/A
ImageJ	Schneider et al., 2012	https://imagej.nih.gov/ij/
CFX Manager 2.1	Bio-Rad	N/A
RNAplfold (ViennaRNA package version 2.3.1)	Lorenz et al., 2011	https://www.tbi.univie.ac.at/RNA/
RNAsubopt (ViennaRNA package version 2.3.1)	Lorenz et al., 2011	https://www.tbi.univie.ac.at/RNA/

RESOURCE AVAILABILITY

Lead Contact

Further information and requests for resources and reagents should be directed to and will be fulfilled by the Lead Contact, Howard Lipshitz (howard.lipshitz@utoronto.ca).

Materials Availability

Materials generated for this study are available on request from Howard Lipshitz (howard.lipshitz@utoronto.ca).

Data and Code Availability

The raw data associated with the mass spectrometry experiments presented in this study have been deposited to the ProteomeXchange Consortium (http://www.proteomexchange.org/). Embryo developmental proteome (deposited via the PRIDE partner repository) with accession number ProteomeXchange: PXD016523; GFP-SLMB and Muskelin-GFP IP-MS (deposited via the PRIDE partner repository) with accession number ProteomeXchange: PXD018794; FLAG-SMG IP-MS (deposited via the MassIVE partner repository) with accession number ProteomeXchange: PXD019280.

Source data used for analyses in Figures 1A and 1D in the paper are available from Casas-Vila et al., 2017 Table S11; https://doi.org/10.1101/gr.213694.116. Source data used for analyses in Figures 1E–1H are available from Eichhorn et al. (2016) Supplementary File 2; https://doi.org/10.7554/eLife.16955.

EXPERIMENTAL MODEL AND SUBJECT DETAILS

Drosophila melanogaster strains were cultivated under standard laboratory conditions at 25°C unless otherwise indicated. 'Wild-type' strains included Canton S and w^{1118}. Strains for GFP IP-MS experiments were: *UAS:GFP-Slimb-6/CyO* (gift from Daniel St Johnston, Cambridge); *w*; P{UAS-muskelin.GFP}attP2* (Bloomington *Drosophila* Stock Center [BDSC] #65860); *nos-GAL4: w^{1118}; P{GAL4::VP16-nos.UTR}CG6325MVD1* (gift from Martine Simonelig, Montpellier; BDSC #4937). RNAi strains against mRNAs encoding proteins of interest were from the Transgenic RNAi Project (TRiP) and were obtained from BDSC: Muskelin (#51405), RanBPM (#61172), CG3295 (#61896), CUL1 (#36601), SKPA (#32991), SLMB (#33898). mCherry RNAi was used as control (gift from T. Hurd; BDSC #35785). The maternal-GAL4 driver used was y^1 *w*; P{matalpha4-GAL-VP16}67; P{matalpha4-GAL-VP16}15* (BDSC #80361). Flies expressing FLAG-tagged SMG transgenes were generated in this study (See Method Details) and crossed to the smg^{47} deletion mutant strain (Chen et al., 2014).

Embryos used for experiments were collected and aged at 25°C unless otherwise indicated. Cages containing male and female adult *Drosophila* were set up with apple juice agar plates supplemented with yeast paste. For unfertilized egg collection, unmated females were used, and males were housed in an adjacent cage, separated by mesh, to promote egg laying. Flies were allowed to acclimatize in cages for at least one day prior to embryo collection, and plates were changed once in the morning and once in the evening to ensure proper developmental staging. After egg lay and development to the desired age on the apple juice agar plates, embryos were harvested for further processing and experiments.

METHOD DETAILS

Embryo developmental proteome

Embryo collection

Each sample of ~300 w^{1118} embryos was collected over a period of 1 hour at 22°C, then aged to the desired stage at the same temperature: (1) as early as possible – sample was not aged, the median time of this collection was defined as 0 min (2) Cycle 14 – 190 min; (3) germ-band extension – 330 min; (4) germ-band retraction – 630 min; and (5) trachea filling – 1290 min. Excess yeast and any dead flies were removed from the surface of the plates. The embryos were dechorionated with 2.5% sodium hypochlorite (50% bleach) solution for 1 min, filtered through a nylon mesh and rinsed under water for 2 minutes to wash off the chorions. Embryos on the mesh were manually counted under the stereo microscope then transferred to a 1.5mL tube containing ~100 μL PBST (1x PBS containing 0.1% Tween-20). All stages were confirmed by visualizing a random sample of ~30 embryos under the stereo microscope (Zeiss Stemi 2000) in halocarbon 27 oil. The embryos were spun down using a mini-centrifuge, and the excess PBST was removed. The embryos were then flash frozen in liquid nitrogen until lysis.

Embryo lysis and MS sample preparation

Sample was prepared as detailed previously (Gupta et al., 2018). Each condition (corresponding to different stages) was lysed in ~150 μL 7M Urea, 2M Thiourea, 2% Sodium dodecyl sulfate (SDS), 1 tablet per 10ml Protease inhibitor (88666, Thermo Fisher), 5mM Dithiothreitol (DTT) and 50mM HEPES(4-(2-hydroxyethyl)-1-piperazineethanesulfonic acid), pH7.2. The embryos were lysed by tip-sonication (FB50, Fisher Scientific): 10 pulses with 10 s on, 20 s off (on ice) at 50% amplitude. Disulfide bonds were reduced by adding 5mM DTT and incubating in a 60°C water bath for 20 minutes. The Cysteines were then alkylated by adding 15mM N-Ethylmaleimide (NEM) and incubating for 20 minutes at room temperature. The alkylation reaction was stopped by adding 5mM DTT and incubating for 10 minutes at room temperature. Salts, small molecules, and lipids were removed by methanol-chloroform precipitation. The resulting protein pellet in each condition was dissolved in 90 μL 6M Guanidine hydrochloride (GuHCl) in 10mM EPPS (4-(2-Hydroxyethyl)-1 piperazinepropanesulfonic acid), pH 8.5. The protein concentration was determined to be 1.7 mg/mL using Pierce BCA Protein Assay Kit (Thermo Scientific). The sample was diluted to 2M GuHCl with 10mM EPPS pH 8.5 and digested overnight at room temperature with 10ng/μL LysC (Wako, 2 μg/μL stock in HPLC-treated water). The sample was further diluted to 0.5M GuHCl with 10mM EPPS pH 8.5. 10ng/μL LysC and 20ng/μL Trypsin (Promega) was added to the samples, which were then incubated at 37oC for 24 hours.

The samples were vacuum concentrated and resuspended in 90 μL of 20mM EPPS pH8.0. The conditions were labeled with 126 (0 h), 127c (3.2 h), 128c (5.5 h), 129c (10.5 h) and 131 (21.5 h) TMT respectively by adding 40 μL of TMT reagent. All the conditions carrying the identification barcode were combined and vacuum concentrated to remove Acetonitrile (ACN). The sample was further acidified with 5% Phosphoric acid. Salts and undigested proteins were removed using C18 Sep-Pak (Water Corporations, 50 mg 1.3 mL column volume). The sample was eluted with 1mL of 70% ACN and 1% formic acid and then was further vacuum concentrated to remove acetonitrile. 10 μg of sample was taken up in 1% formic acid and 1 μg of that was analyzed on the mass spectrometer to confirm the quality of digestion and labeling.

The rest of each sample was resuspended in 450 μL of 10mM ammonium bicarbonate pH 8.0, 0.5% ACN and then pre-fractionated by medium pH reverse-phase HPLC using a flow rate of 0.5mL/min throughout. The gradient was 0% ACN for 18 minutes, then 7% to 35% ACN for 57 minutes, and then a flat gradient of 95% ACN for 5 minutes. Throughout prefractionation the pH was buffered with 10mM ammonium bicarbonate, pH 8.0. The fractions were collected using a fraction collector (Agilent 1260 Infinity) into a 96 well plate. The 96 fractions were pooled into 24 fractions by combining the alternating well from each column of the plate. Each fraction

was vacuum concentrated and resuspended in 50 μL of 5% phosphoric acid. Stage-tip was performed to desalt the sample, and the sample was resuspended in 6 μL of 1% formic acid. 1.5 μL was analyzed by LC-MS.

HPLC and MS

The instrument was equipped with an Easy nLC 1200 high pressure liquid chromatography (HPLC) pump. For each run, peptides were separated on a 100 μm inner diameter microcapillary column, packed first with approximately 0.5 cm of 5μm BEH C18 packing material (Waters) followed by 30 cm of 1.7μm BEH C18 (Waters). Separation was achieved by applying a 6%–30% ACN gradient in 0.125% formic acid and 2% DMSO over 90 min at 350 nL/min at 60°C. Electrospray ionization was enabled by applying a voltage of 2.6 kV through a microtee at the inlet of the microcapillary column.

The Orbitrap Fusion Lumos used the TMTc+ method (Sonnett et al., 2018). The mass spectrometer was operated in data-dependent mode with a survey scan ranging from 500-1400 m/z at resolution of 120k (200 m/z). 10 most intense ions for CID MS2 fragmentation using the quadrupole. Only peptides of charge state 2+ were included. Dynamic exclusion range was set to 60 s with mass tolerance of 10ppm. Selected peptides were fragmented using 32% HCD collision energy, and the resultant MS2 spectrum was acquired using the Orbitrap with a resolution of 60k and 0.4 Th isolation window.

Primary antibody generation

Anti-eIF4E and anti-CG3295 antibodies were raised in rat (Eurogentec). Antigens were prepared as follows: eIF4E1 IsoformA was expressed in *E. coli* as a His6-SUMO fusion protein. After metal affinity chromatography, the N-terminal SUMO domain was cleaved off with ULP protease, and the two protein fragments were separated by a second metal affinity column. CG3295 was expressed in *E. coli* as a His6 fusion protein. The protein was purified from inclusion bodies under denaturing conditions via metal affinity chromatography.

Western blotting

Primary antibodies used were: Guinea pig anti-SMG (1:20000), rabbit anti-SMG (1:500), rat anti-Cup (1:10000), rabbit anti-Cup (1:1000), rabbit anti-TRAL (1:5000), rat anti-TRAL (1:1000), rabbit anti-ME31B (1:1000 Figure 2; 1:5000 others), rabbit anti-BEL (1:2000), Guinea pig anti-SLMB (1:4000), rat anti-CG3295 (1:500), rat anti-eIF4E (1:1000). Mouse anti-Tubulin (1:25000 Figure 2; 1:20000 others) or mouse anti-Actin (1:1000) were used as loading controls.

For the developmental western blots shown in Figures 2 and S2, embryos were collected, dechorionated for 30 s in 12% sodium hypochlorite, weighed, homogenized in SDS sample buffer with a pestle and boiled for 5 min. Proteins were resolved by SDS-PAGE and transferred to a nitrocellulose membrane. Blots were blocked at room temperature with 1.5% cold water fish gelatin (Sigma) in TBS for 1 hour, then incubated with primary antibodies diluted in 1.5% gelatin in TBST (TBS plus 0.05% Tween 20) at 4°C overnight. Subsequently, blots were washed 5 × 6 minutes with TBST at room temperature and incubated with the appropriate fluorescently labeled secondary antibodies (1:15000, Li-COR) in TBST at room temperature for 2 hours. Blots were washed 5 × 6 minutes with TBST, imaged using an Odyssey CLx scanner and Image Studio Lite software (LI-COR) and band intensities were quantified using ImageJ.

For all other western blots, dechorionated embryos were counted, then lysed in SDS-PAGE sample buffer at a concentration of 1 embryo/μL and boiled for 2 minutes. Proteins were resolved by SDS-PAGE and transferred to PVDF membrane. Blots were blocked at room temperature with 2% non-fat milk in PBST for 30 minutes and incubated with primary antibodies diluted in 2% non-fat milk in PBST at 4°C overnight. Subsequently, blots were washed 3 × 10 minutes with PBST at room temperature and incubated with the appropriate HRP-conjugated secondary antibodies (1:5000, Jackson ImmunoResearch) in 2% non-fat milk in PBST at room temperature for 1 hour. Blots were washed 3 × 15 minutes with PBST and developed using Immobilon Luminata Crescendo Western HRP substrate (Millipore), imaged using ImageLab (BioRad) and band intensities were quantified using ImageJ.

MG132 treatment

1–2 hour old embryos were permeabilized using a modification of a published method (Rand et al., 2010): Embryos were dechorionated for 30 s in 12% sodium hypochlorite. 45.25 mL of Modified Basic Incubation Medium (MBIM) (Strecker et al., 1994) was mixed with 0.25 mL Triton X-100 and 4.5 mL (R)-(+)-limonene (Merck), the dechorionated embryos were incubated with this mix for 30 s and then washed extensively with PBS followed by PBS/0.05% Tween 20. They were then incubated in MBIM containing 100 μM MG132 + 0.05% DMSO or 0.05% DMSO only, for 3 hours at 25°C, washed in PBS, lysed in SDS-PAGE loading buffer, and analyzed by western blot.

FLAG-SMG transgenes

For generation of transgenic flies expressing FLAG-SMG and FLAG-SMG767Δ999, the base vector used was the *smg5′UTR-BsiWI-smg3′UTR* (*SBS*) plasmid (Tadros et al., 2007). A linker carrying a start codon, the FLAG/p53 epitope tags, and *Asc*I and *Pme*I restriction sites was inserted into the *Bsi*WI site of *SBS*, between the *smg* UTRs. Genomic sequences of corresponding transgenic *smg* proteins were inserted between the *Asc*I and *Pme*I sites. Coding sequence for amino acids 1–999 (for expression of full-length FLAG-SMG) and for amino acids 1–766 (for expression of truncated FLAG-SMG767Δ999) were amplified from a *smg* genomic rescue construct (Dahanukar et al., 1999) using a 5′-primer with an *Asc*I linker and a 3′-primer with a *Pme*I linker. The ORFs were inserted between the *Asc*I and *Pme*I sites in the SBS plasmid. *smg* genomic transgenes were then inserted into a pCaSpeR4 cloning vector

with an attB site (Markstein et al., 2008; Tadros et al., 2007). Transgenic *smg* constructs were integrated into an attP40 landing site on the second chromosome (2L:25C7) (Markstein et al., 2008) by Genetic Services (Cambridge, MA) using phiC31, a site-specific integrase (Groth et al., 2004). The inserted transgenes were then crossed into a smg^{47} mutant background (Chen et al., 2014).

FLAG IP-MS

Immunoprecipitation

For FLAG-SMG IP-MS experiments, 0–3 hour old embryos were collected from flies expressing FLAG-SMG, FLAG-SMG767Δ999 or non-transgenic w^{1118} flies as control. Dechorionated embryos were crushed in a minimal volume of lysis buffer (150 mM KCl, 20 mM HEPES-KOH pH 7.4, 1 mM MgCl2, 0.1% Triton X-100, supplemented with protease inhibitors and 1 mM DTT), cleared by centrifugation for 15 minutes at 4°C and 20,000 x g, and stored at −80°C. Immediately prior to IP, the lysate was diluted twofold with lysis buffer and cleared again by centrifugation. Protein concentration was measured by Bradford Assay (Bio-Rad), and samples were adjusted with lysis buffer to equal concentrations. For each IP, 500 μL of diluted lysate, with or without 350 μg/mL RNase A, was mixed with 20 μL of anti-FLAG M2 beads (Sigma; blocked with 5mg/mL BSA) or Protein A beads as control, then incubated for ~3 hours at 4°C with end-over-end rotation. After incubation, beads were washed 4–5 times with lysis buffer, twice with lysis buffer lacking Triton X-100, then transferred to new tubes, and washed twice with lysis buffer lacking Triton X-100.

Sample preparation

Bound proteins were eluted by tryptic digest: beads were resuspended in 200 μL of 50 mM ammonium bicarbonate, pH 8, with 2 μg of trypsin (Pierce), and incubated overnight at room temperature with end-over-end rotation. The digested supernatant was recovered, and beads were washed once with an additional 200 μL of 50 mM ammonium bicarbonate. The two eluates were pooled and dried by Speed-vac. Samples were desalted with C18 tip (Pierce C18 Spin Tips, Thermo Scientific cat. no. 84850) following the manufacturers' protocol and dried by Speed-vac. Samples were then resuspended in 26 μL of 1% (vol/vol) formic acid, and centrifuged at 13,200 RPM for 20 minutes. 22 μL was loaded into a 96 well plate, two 10 μL injections were made for each sample.

HPLC and MS

For liquid chromatography the following solvents were used: Solvent A (0.1% (vol/vol) formic acid) and Solvent B (0.1% (vol/vol) formic acid/90% (vol/vol) acetonitrile). LC solvents were replaced a minimum of every 2 weeks. The LC parameters were set up using an Easy-nLC 1200 instrument. Peptides were loaded and separated on a nanoViper trap column (75 μm x 2 cm), Acclaim PepMap 100 (C18, 3 μm, 100 Å, Thermo Scientific, cat. no. 164946) and EASY-Spray analytical column (75 μm x 50cm) Acclaim PepMap RSLC (C18, 2 μm, 100Å, Thermo Scientific) at a flow rate of 225nL/min. Tandem MS was performed using the Q Exactive HF-Orbitrap mass spectrometer (Thermo Scientific), as previously described (Chiu et al., 2016; Jiang et al., 2015; Liu et al., 2014; Mirali et al., 2020). The parameters for acquisition were 1 MS scan (50 ms; mass range, 390 to 1800) at a resolution of 60,000K, followed by up to 20 MS/MS scans (50 ms each) at a resolution of 15,000 and an AGC target of $1x10^5$. Candidate ions with charge states +2 to +7 were isolated using a window of 1.4 amu with a 5 s dynamic exclusion window.

GFP IP-MS

Immunoprecipitation and sample preparation

For GFP-tagged proteins, 0–2 hour old embryos were collected from flies expressing either GFP-SLMB, Muskelin-GFP or from non-transgenic Canton S flies as control. Embryos were dechorionated for 30 s in 12% sodium hypochlorite and lysed in 50 mM Tris pH 7.5, 150 mM sodium chloride, 1% NP-40, 0.5% sodium deoxycholate and protease inhibitor mix, by homogenization with a pestle on ice. The extract was cleared by centrifugation (20000 x g, 4°C), frozen in liquid nitrogen and stored at −80°C. The lysate was treated with RNase A (100 μg/ml) for 10 min at room temperature, cleared again by centrifugation (20000 x g, 4°C) and diluted 1:5 with GFP wash buffer (50 mM Tris-HCl, pH 7.5, 150 mM NaCl, 0.5 mM EDTA). The diluted extract was incubated with GFP-Trap matrix (Chromotek, equilibrated in GFP wash buffer) for 1 h at 4°C. The matrix was washed 3 times with GFP wash buffer and resuspended in 8 M urea/ 0.4 M ammonium bicarbonate. Bound proteins were reduced with DTT (7.5 mM, 30 min at 50°C), alkylated with chloroacetamide (20 μL 100 mM per 120 μL reduced sample, 30 min at room temperature), adjusted with water to 800 μL and digested with sequencing grade trypsin (Promega, 1:50 w/w trypsin to protein ratio) at 37°C overnight. Digests were separated from beads by centrifugation and stopped by addition of 40 μL 10% TFA. Samples were concentrated by Speed-vac.

HPLC and MS

Samples were analyzed by LC-MS/MS using a U3000 RSCL nano-HPLC system coupled to an Orbitrap Q-Exactive Plus mass spectrometer with NanoFlex ionization source (all from Thermo Fisher Scientific). Samples were loaded on a trap column (PepMap RP-C18, 300 μm x 5 mm, 5 μm, 100 Å, Thermo Fisher Scientific) with 0.1% TFA at a flow rate of 30 μL/min. After 15 min, peptides were eluted via an in-house packed separation column (self-pack PicoFrits, 75 μm x 50 cm, 15 μm tip, New Objective, packed with ReproSil-Pur 120 C18-AQ, 1.9 μm, Dr. Maisch GmbH). For peptide separation, a linear 180-min gradient was applied (3% - 40% eluent B; eluent A: 0.1% formic acid in water, eluent B: 0.08 formic acid in acetonitrile) at a flow rate of 230 nL/min. Data were acquired using a data-dependent top10 strategy (one MS survey scan, followed by 10 MS/MS scans of the 10 most abundant signals). MS data (m/z range 375-1800) were recorded with R = 140,000 at m/z 200, MS/MS data (HCD, 28% normalized collision energy) with R = 17,500 at m/z 200.

Maternal RNAi knockdown

Females expressing the maternal-Gal4 driver (BDSC #80361) were crossed to males expressing UAS-hairpin RNA targeting each gene assayed from the TRiP library (see Experimental Model). UAS-hairpin RNA targeting mCherry was used as control knockdown. Adult F1s from these crosses were used for embryo collection. Maternal knockdown efficiency was assayed in 0–3 h embryos by RT-qPCR. In the case of *slmb* RNAi, depletion of *slmb* mRNA was incomplete; knockdown was, therefore, further validated by western blotting.

RT-qPCR

Total RNA was collected from dechorionated embryos in TRI Reagent (Sigma) following the manufacturer's protocol. 500 ng of total RNA per sample was used to synthesize cDNA with Superscript IV reverse transcriptase kit (Invitrogen) and the reaction was primed using random hexamers. The resultant reaction containing single-stranded cDNA was diluted 1:20 with RNase-free water and used for quantification by qPCR. Primers specific to the transcripts assayed were designed using NCBI Primer-BLAST to cover all isoforms and span an exon-exon junction (Table S6). Quantitative real-time PCR was performed on a CFX384 Real-Time System (Bio-Rad), using Sensifast SYBR PCR mix (Bioline) following the manufacturer's protocol and using 5 μL of diluted cDNA per reaction. Expression of each gene was averaged across three technical replicates per biological replicate and normalized to *RpL32* control.

Immunostaining

0–3 hour old embryos were collected from F1 adults from maternal RNAi crosses, dechorionated with 4.2% sodium hypochlorite for 2 minutes, then fixed in 4% formaldehyde and heptane for 20 minutes, and devitellinized by the addition of methanol and vigorous shaking. Fixed embryos were rehydrated by washing 4 times with PBSTx (PBS, 0.1% Triton X-100) and blocked with 10% bovine serum albumin (BSA) in PBSTx. Embryos were incubated with guinea pig anti-SMG (1:2000 dilution, 1% BSA in PBSTx) rocking overnight at 4°C and subsequently washed 3 × 15 minutes while rocking at room temperature. Embryos were then incubated in Cy3-conjugated donkey anti-guinea pig secondary antibody (1:300 dilution, 1% BSA in PBSTx; Jackson ImmunoResearch) for 1 hour rocking at room temperature, and washed 5 × 10 minutes with PBSTx. 0.001 mg/mL DAPI (Sigma) was added to the second wash to label DNA. Embryos were mounted in 2.5% DABCO (Sigma), 70% glycerol in PBS. Images were collected using a Zeiss AxioSkop-2 MOT fluorescence microscope and the QCapture Suite PLUS acquisition software.

SMG target-RNA prediction

To computationally predict the formation of SMG recognition element (SRE) stem/loops ($CNGGN_{0-4}$ loop sequence on a non-specific stem) within a transcript, we used a multi-step pipeline modified from our previous method (Chen et al., 2014). Each transcript was first scanned with RNAplfold (ViennaRNA package version 2.3.1) using the parameters -W = 170 -L = 120 -T = 25 (Lange et al., 2012). Next, the transcript was scanned for CNGG motif (and variant motif) sites, and if the RNAplfold results indicated that the base immediately 5′ to the motif formed a base-pair interaction with one of the five nucleotides immediately 3′ to the motif with a probability > 0.01, then the motif was marked for further analysis. The probability of stem/loop formation at each site was then assessed with RNAsubopt using a 120nt sliding window that overlapped the candidate site (the first window beginning at 75nt upstream of the motif and extending 40nt downstream of the motif, which was shifted by one nucleotide in the 3′ direction per window 34 times for a total of 35 windows), for which 3000 structures were sampled per window. The empirical probability of stem/loop formation for each site was averaged across the 35 windows and expressed as a percentage to produce a score for each motif; scores from individual motifs were then summed across the entire transcript to produce the final SRE score for the whole transcript. Zygotic targets not likely to be potential SMG targets had SRE scores < 5. All SMG-bound targets assayed had SRE scores > 10.

QUANTIFICATION AND STATISTICAL ANALYSIS

Embryo developmental proteome

A suite of software tools developed in the Gygi Lab was used to convert mass spectrometric data from the Thermo RAW file to the mzXML format, as well as to correct erroneous assignments of peptide ion charge state and monoisotopic m/z (Huttlin et al., 2010; Sonnett et al., 2018). We used RawFileReader libraries from Thermo, version 4.0.26 to convert the raw files into mzXML file format. Assignment of MS2 spectra was performed using the SEQUEST algorithm v.28 (rev. 12) by searching the data against the appropriate proteome reference dataset acquired from UniProt (*Drosophila melanogaster* with Proteome ID UP000000803, Protein count 21988 downloaded in July, 2017; *Saccharomyces cerevisiae* (yeast) with Proteome ID UP000002311, Organism ID 9606, Protein count 6049 downloaded in July, 2017) including 114 common contaminants like human Keratins and Trypsin. The MS spectrum to peptide mapping can be found on ProteomeXchange: PXD016523. This forward database component was followed by a decoy component which included all listed protein sequences in reversed order (Elias and Gygi, 2007). Searches were performed using a 20-ppm precursor ion tolerance, where both peptide termini were required to be consistent with Trypsin or Lys-C specificity, while allowing one missed cleavage. Fragment ion tolerance in the MS2- spectrum was set at 0.02 Th. NEM was set as a static modification of cysteine residues (+125.047679 Da), TMT as a static modification of lysine residues and peptides' N-termini (+229.162932 Da), oxidation of methionine residues (+ 15.99492 Da) as a variable modification. An MS2 spectral assignment false discovery rate of 0.5% was achieved by applying the target decoy database search strategy. Filtering was performed using a Linear Discriminant analysis with the following

features: SEQUEST parameters XCorr and unique Δ XCorr, absolute peptide ion mass accuracy, peptide length, and charge state. Forward peptides within three standard deviations of the theoretical m/z of the precursor were used as positive training set. All reverse peptides were used as negative training set. Linear Discriminant scores were used to sort peptides with at least seven residues and to filter with the desired cutoff. Furthermore, we performed a filtering step on the protein level by the ''picked'' protein FDR approach (Savitski et al., 2015). Protein redundancy was removed by assigning peptides to the minimal number of proteins that could explain all observed peptides, with the above-described filtering criteria. TMTc+ data were analyzed as previously described (Sonnett et al., 2018a, 2018b). To correct for pipetting errors in the experiments, we normalized the signal such that the median peptide ratio between all the stages was 1:1:1:1:1.

Assigning confidence intervals to the development proteome

We used BACIQ **(B**ayesian **A**pproach to **C**onfidence **I**ntervals for protein **Q**uantitation) (Peshkin et al., 2019) to assign confidence to the relative expression of proteins at each developmental stage (https://github.com/wuhrlab/BACIQ). Specifically, we used the model version that shares the variances across all proteins. To obtain the most probable estimates and the confidence associated with a protein's expression at a stage, we fed the algorithm with the ions corresponding to that stage and the total ion counts in all other stages for all the underlying peptides of the given protein. To convert the peptide Signal/FT-noise signal into counts, a multiplicative factor of 2.1 (for 30k Orbitrap resolution) was used. The algorithm outputs the posterior distribution for the relative expression for every protein. The estimate is the median of the distribution and the confidence is given by 95% intervals.

Estimated rank ordering of protein abundances

To estimate the rank-ordering of protein abundance we followed a procedure previously described (Wühr et al., 2014). We integrated each PSMs raw signal in MS1 over time with 10ppm tolerance using the GFY software licensed from Harvard University. The number of ions per PSM were summed for all PSMs that matched a protein, then normalized to the number of theoretically calculated tryptic peptides, with at least 7 and maximally 25 amino acids (missed cleavages were not allowed for theoretical peptides). We rank-ordered estimated protein abundances by this normalized integrated signal.

k-means clustering

k-means clustering was performed using the kmeans function in MATLAB 2019a with ''Replicates'' set to 30. The number of clusters was selected to 6 to capture overall protein dynamics. Further cluster increases did not reveal new cluster dynamics.

Comparison of proteome to transcriptome datasets

Cluster 4 and Cluster 6 proteins in the embryo proteome presented in this study were each compared to the transcriptome and translatome (ribosome-association) previously published in Eichhorn et al. (2016). Scatterplots of these comparisons are presented in Figures 1E–1H. For consistency between datasets, genes associated with all transcripts analyzed were converted to FlyBase Gene IDs (FBgn) from FlyBase release 6.30. For each comparison, only genes expressed in both datasets were included in the scatterplots and statistical analyses. Proteins mapping to multiple genes were excluded. Minimum RPKM expression was set to 0.01, and minimum TE was set to 0.001 to avoid dividing by zero. Relationship between change in protein abundance and either change in transcript abundance or change in translation efficiency were determined statistically using Fisher's exact test. For genes in Cluster 4, proportion of proteins with $\geq$ 2-fold increase in RNA level (Figure 1E) or $\geq$ 2-fold increase in translation efficiency (Figure 1G) within the cluster were compared to their respective proportions within the entire proteome. For genes in Cluster 6, similar analyses were performed for $\geq$ 2-fold decrease in protein level with the corresponding transcript's decreases in RNA level (Figure 1F) or translation efficiency (Figure 1H). *P* values for these associations are presented in the relevant figure panels, figure caption, and described in detail in the text.

Gene set enrichment analysis

Gene Ontology (GO) term enrichment analyses were carried out using the DAVID functional annotation tool online at https://david.ncifcrf.gov/ (Huang et al., 2009a, 2009b). Genes in each of the six clusters were analyzed against the background list of all expressed genes through all time points. For each cluster, Level 3 terms were selected for each of the 'molecular function', 'cellular component' and 'biological process' categories. For Cluster 6, Level 4 terms were subsequently selected to obtain more refined GO terms. A Benjamini *P*-value cut-off of 0.1 was used to report significantly enriched GO terms.

Motif discovery

Multiple Em for Motif Elicitation (MEME) (Bailey and Elkan, 1994) was used through The MEME Suite 5.1.1 at http://meme-suite.org/. Protein sequences were downloaded from UniProtKB. Motif discovery was performed in the discriminative mode using all 154 Cluster 6 proteins as primary sequences and either 2595 proteins, representing most of Cluster 1, or 394 RNA-binding and RNP-associated proteins within Cluster 1 as control sequences. Settings used specified up to 10 motifs of 4-12 residues in length. Motifs with E-value $\leq 10^{-4}$ are presented in Figure S1.

FLAG IP-MS

Biological replicates of FLAG IP-MS represent pull-downs performed on embryo lysate from independently collected embryo populations. For FLAG-SMG IP, four biological replicates were performed without RNase treatment, five biological replicates with RNase treatment. Two types of negative controls were used: Protein A IP from the same lysate expressing FLAG-SMG (two replicates), or FLAG pull-down from wild-type (w^{1118}) embryo lysate (three replicates). The set of five control IPs was performed with or without RNase, and controls and IPs matching the same treatment conditions were used for analysis.

The ProHits software package (Liu et al., 2010) was used to perform peptide validation and protein interaction analysis. Proteins with associated peptide counts were filtered through the Trans Proteomic Pipeline (TPP) for iProphet probability > 0.95 and number of unique peptides $\geq$ 2 (Shteynberg et al., 2011). Significance Analysis of INTeractome (SAINT) was used to determine the probability of each interacting protein (Choi et al., 2011). SAINTexpress was run on the ProHits interface using number of compressed controls = 3; nburn = 2000; niter = 5000; lowMode = 1; minFold = 1; normalize = 1; no bait compression. The average iProphet peptide counts for detected proteins in our FLAG-SMG IPs are presented in scatterplots in Figures 3A and 3B. For interacting proteins not detected in the negative control, average peptide count in the control IP is plotted as 0.1 (small number) to avoid taking the log of zero. Bayesian false discovery rates (BFDRs) from SAINT analysis for proteins of interest are also annotated in the figure panels and figure captions. A comprehensive list of peptide counts for each replicate, SAINT scores, and BFDR for all captured proteins can be found in Table S4.

Three biological replicates of FLAG-IP from embryos expressing FLAG-SMG767Δ999 were performed in parallel with three replicates of FLAG-SMG IPs and control (w^{1118}) IPs, each treated with 350 μg/mL of RNase A. MS results from these FLAG-SMG767Δ999 IPs and control IPs were analyzed using the methods described above to determine interactors that were lost upon truncation of the SMG C terminus. Peptide counts, fold enrichment and SAINT analysis of interactors with SMG767Δ999 can be found in Table S4.

GFP IP-MS

Biological replicates of GFP IP-MS represent IPs performed on embryo lysate from independently collected embryo populations. Three biological replicates were performed for each genotype: embryos expressing Muskelin-GFP, embryos expressing GFP-SLMB, and wild-type (Canton S) embryos as negative control.

MS data were analyzed with MaxQuant 1.6.1.0 with label-free quantification (Cox and Mann, 2008). The modification parameter was set according to the alkylation reagent used, iBAQ values were reported and the different runs of an experiment were matched if applicable. Average iBAQ intensities for proteins detected in the GFP-IPs versus control IPs are presented as scatterplots in Figures 3C and 3D. For interacting proteins not detected in the negative control, average peptide count in the control IP is plotted as 10 (small number) to avoid taking the log of zero. *P*-values were calculated with a one-tailed, unpaired Student's t test. *P*-values are annotated for protein interactors of interest in the figure panels and figure captions. A comprehensive list of iBAQ intensities for each replicate, fold enrichment and *P*-values for all captured proteins can be found in Table S5.

Determination of ubiquitination sites

For determination of ubiquitination sites the MS raw data (Götze et al., 2017) were reanalyzed with Proteome Discoverer 2.4 (Thermo Fisher Scientific) using Sequest HT and MS Amanda 2.0 for database search against the amino acid sequences of TRAL, ME31B, SMG, Cup and Muskelin setting GG modification of lysines as variable modification. False discovery rates (FDRs) were determined by a target decoy approach. Only GG-modified peptides identified by both search engines Sequest HT and MS Amanda with high confidence (FDR < 0.01) were considered as unambiguously ubiquitinated. Ubiquitination of these peptides was further confirmed by inspection of the relevant spectra. Analysis of ubiquitinated peptides is presented in Table S3.

Quantification of western blots

Developmental western blots (Figures 2A and S2) were quantified using ImageJ. Each protein was normalized to the tubulin loading control, and the highest signal for each was set to 100. For RNAi experiments presented in Figures 4 and 5, protein expression was assayed by western blot. For each knockdown at each time point, lysates equivalent to 10 embryos were run on SDS-PAGE for quantification. Three biological replicates, representing three independent embryo collections were assayed. Band intensities were quantified using ImageJ and normalized to α-Tubulin as loading control. For each replicate, intensities were normalized to the first time point (0-1 hour). Averages of the 3 replicates are presented in these figures with error bars representing standard deviation (Student's t test, two-tailed, unpaired). Significance thresholds are presented in the figures and figure captions.

Quantification of RNA expression

Quantitative real-time PCR (qPCR) data were analyzed using the CFX Manager software (Bio-Rad). For each of three biological replicates, representing three independent embryo collections, values from three technical replicates were averaged and relative gene expression was normalized to the ribosomal protein transcript *RpL32* as control. For gene expression analyses presented in Figure 7, see below. For all other quantification of RNA expression, normalized expression is presented as the average of three replicates with error bars representing standard deviation (Student's t test, two-tailed, unpaired). Significance thresholds are presented in the figures and figure captions.

Gene expression in FLAG-SMG767Δ999

Quantitative real-time PCR (qPCR) data were analyzed using the CFX Manager software (Bio-Rad). Expression of each gene of interest was assayed in two biological replicates per time point per genotype, representing two independent embryo collections of ~50 embryos each. For each biological replicate, values from three technical replicates were averaged and relative gene expression was normalized to the ribosomal protein transcript *RpL32* as control. Expression of each gene was further normalized to the first time point (0-2.5h hours). Mean and standard deviation of normalized expression are presented in Figure 7. For each group of genes (maternal, zygotic, re-expressed), differences in expression between the two genotypes were analyzed using the Wilcoxon signed-rank test. *P*-values for each gene group are presented in Figure 7.

Cell Reports, Volume *31*

Supplemental Information

Precise Temporal Regulation of Post-transcriptional Repressors Is Required for an Orderly *Drosophila* Maternal-to-Zygotic Transition

Wen Xi Cao, Sarah Kabelitz, Meera Gupta, Eyan Yeung, Sichun Lin, Christiane Rammelt, Christian Ihling, Filip Pekovic, Timothy C.H. Low, Najeeb U. Siddiqui, Matthew H.K. Cheng, Stephane Angers, Craig A. Smibert, Martin Wühr, Elmar Wahle, and Howard D. Lipshitz

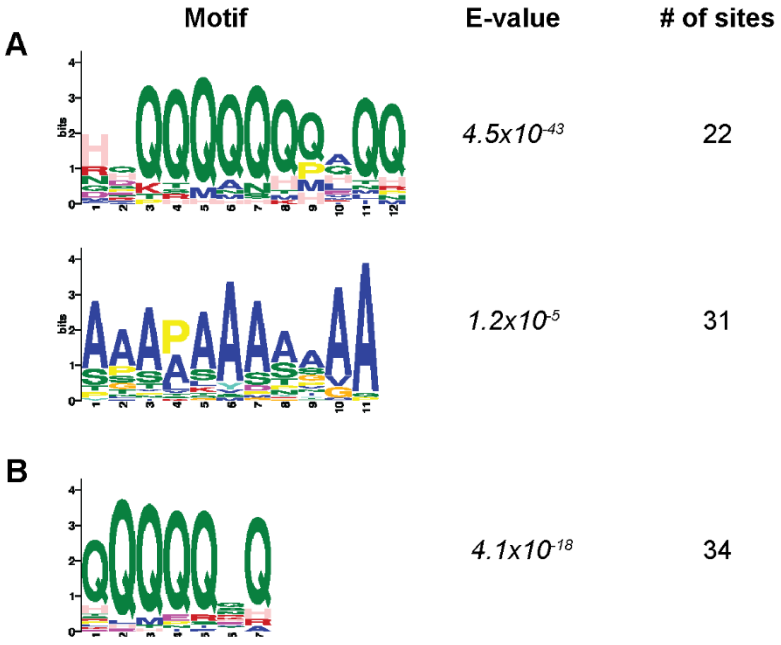

Figure S1. MEME analysis of Cluster 6 proteins reveals enrichment for low complexity regions, related to Figure 1. MEME was performed on all 154 Cluster 6 proteins against **A.** Nearly all proteins from Cluster 1 (2595 sequences), or **B.** All annotated RNA-binding and RNP-associated proteins from Cluster 1 (394 sequences). Motifs with E-value (enrichment significance) $\leq 10^{-4}$ are shown, along with number of sites for each motif within Cluster 6.

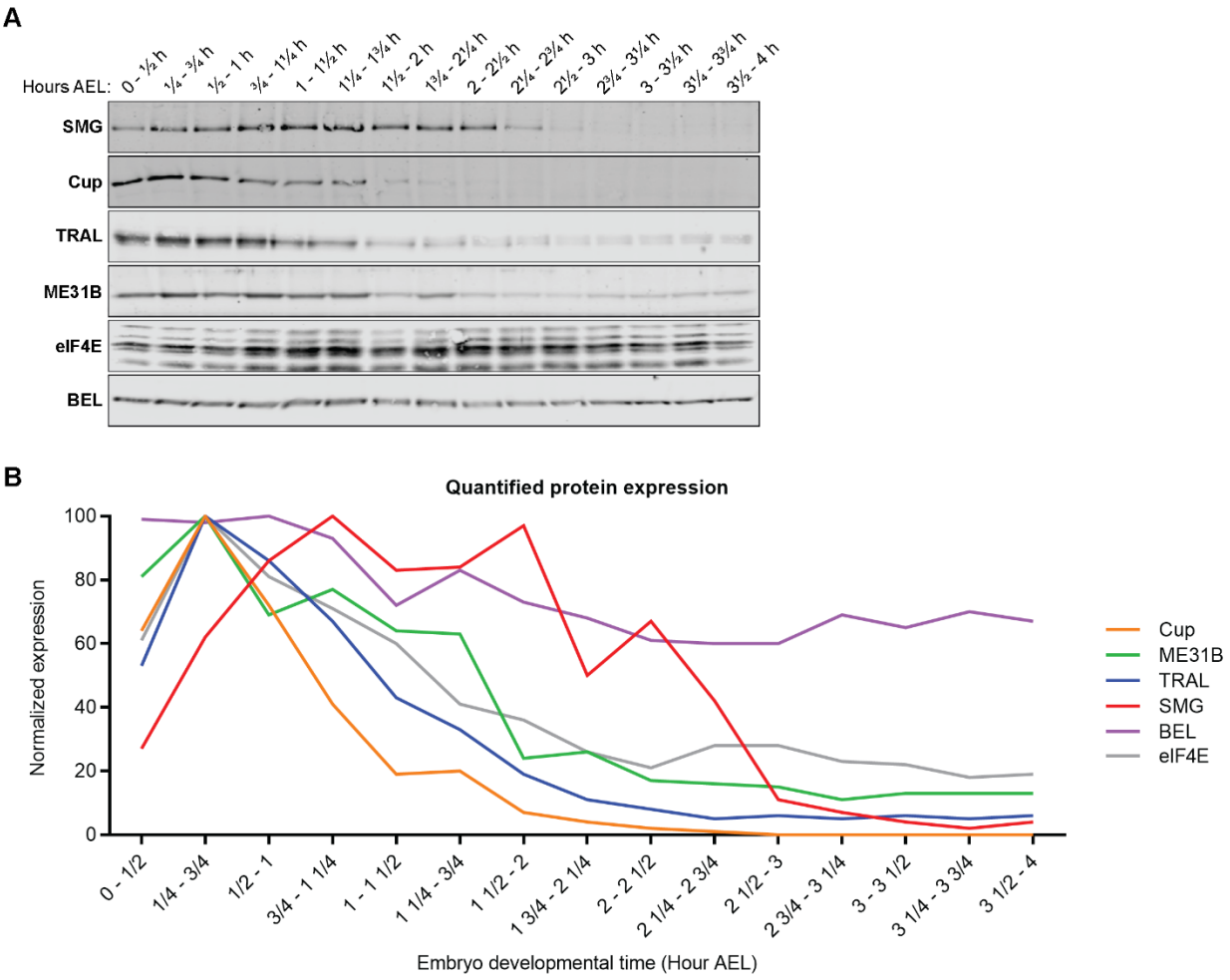

Figure S2. RBP expression is differentially regulated during the MZT, related to Figure 2. **A.** Biological replicate of the developmental Western blot shown in Figure 2A, assayed over the first four hours of embryogenesis after egg lay (AEL). **B.** Quantification of protein expression across 2 biological replicates and at least 2 technical replicates (with the exception that only one sample was quantified for eIF4E). Each protein was normalized to tubulin (see Figure 2, not shown here), and its peak expression during the time course was set to 100.

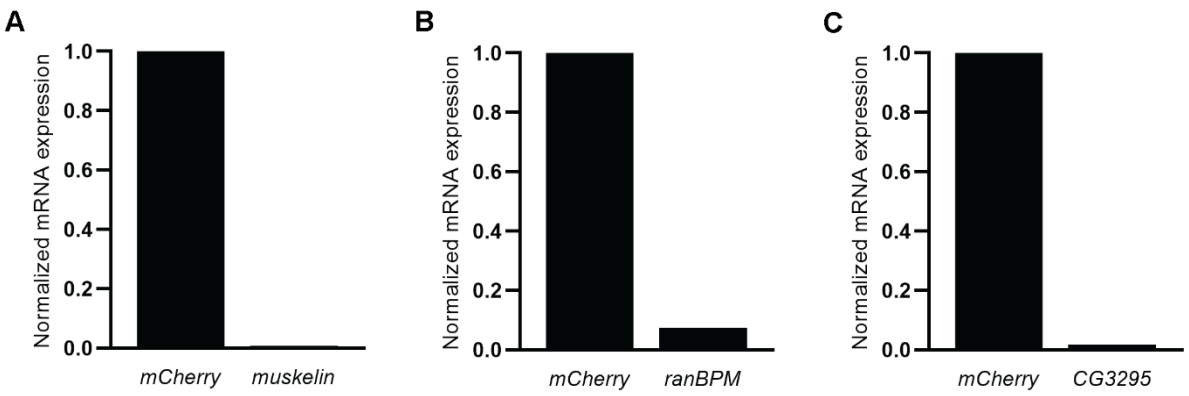

Figure S3. Validation of maternal RNAi knockdown of CTLH complex members, Related to Figure 4. RT-qPCR quantification of target mRNA expression in 0-3h embryos. **A.** *muskelin*, **B.** *ranBPM* and **C.** *CG3295* mRNAs were depleted by > 90% relative to *mCherry* control RNAi in their respective maternal knockdowns.

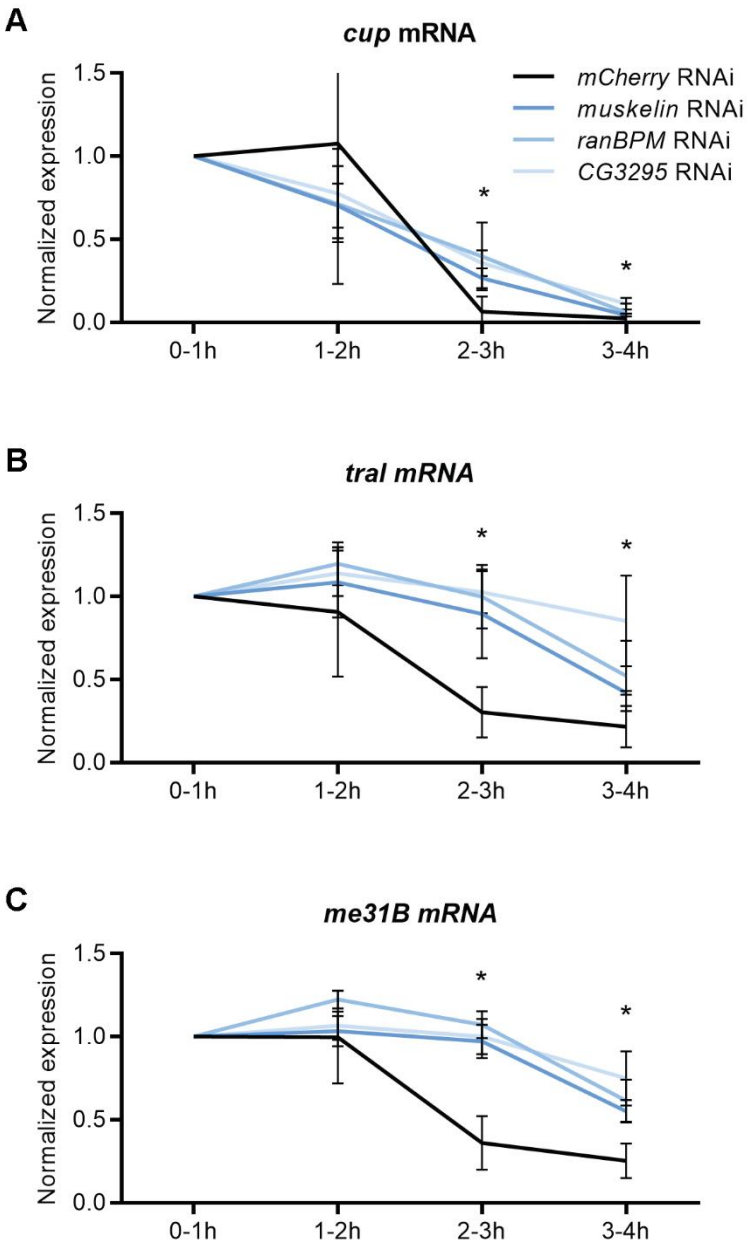

Figure S4. Knockdown of the CTLH complex results in delayed degradation of mRNAs, related to Figure 4. RT-qPCR quantification of mRNA expression in embryos assayed in **Figure 4A-D**. Knockdown of the CTLH complex resulted in delayed degradation of *cup* (**A**), *tral* (**B**) and *me31B* (**C**) mRNA relative to control knockdown. *tral and me31b* remained partially stabilized at 3-4h after egg-lay. *$P < 0.05$, *n.s.* = not significant, n = 3, error bars = SD, Student's *t*-test.

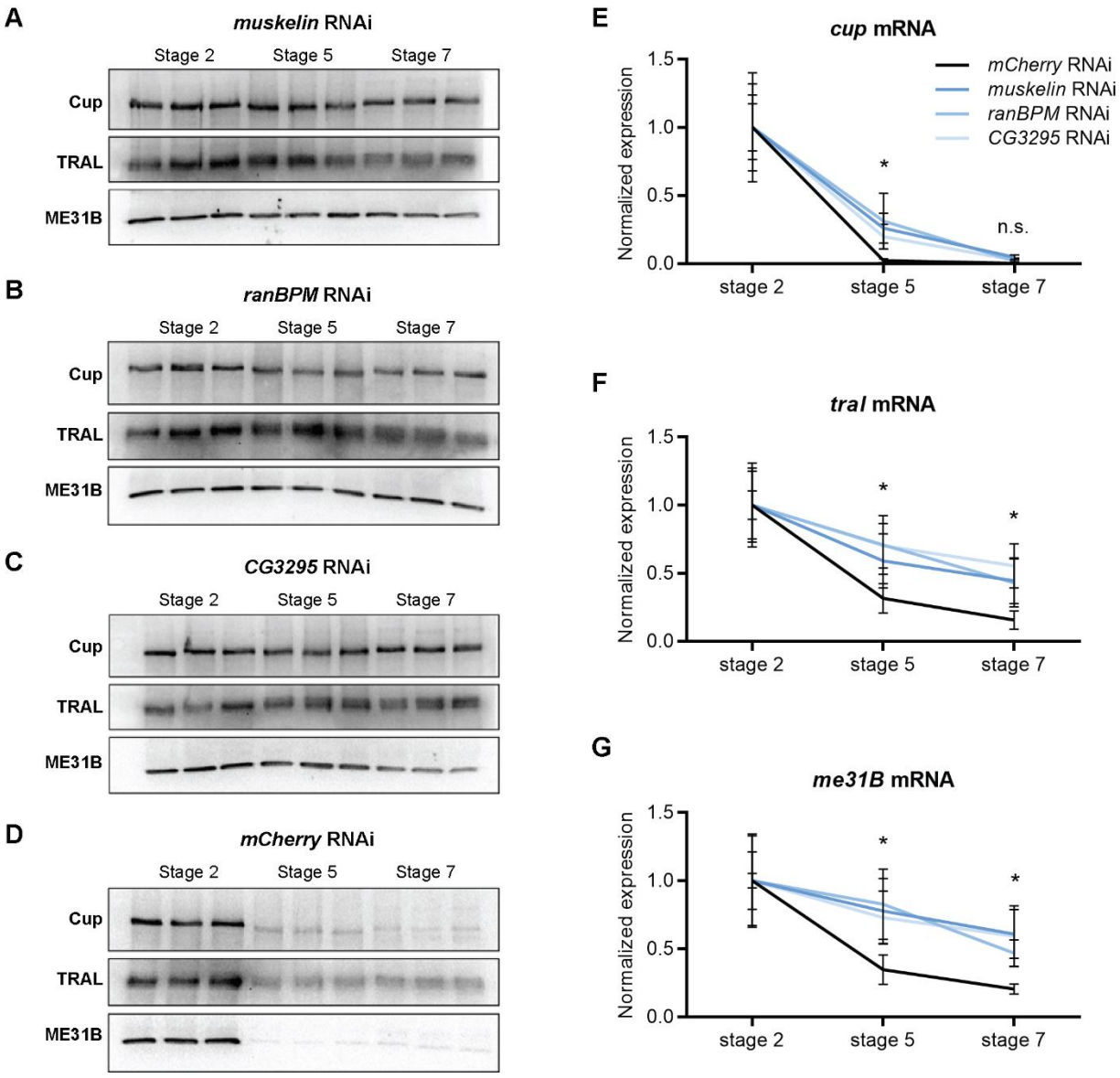

Figure S5. Knockdown of the CTLH complex stabilizes Cup in developing embryos, related to Figure 4. A-D. Western blots of embryos picked at Stage 2, Stage 5 and Stage 7 (n = 3 biological replicates for each stage). Maternal knockdown of *muskelin* (**A**), *ranBPM* (**B**) and *CG3295* (**C**) resulted in stabilization of Cup, TRAL and ME31B through embryo Stage 7, whereas all three RBPs were depleted in the embryo by Stage 5 in the control knockdown (**D**). **E-G.** RT-qPCR quantification of mRNA expression in embryos assayed in A-D. Picking developmentally stage-matched embryos partially rescued the delay in mRNA degradation in CTLH maternal knockdown embryos. *cup* (**E**) was cleared to comparable levels as in control *mCherry* RNAi by stage 7. *tral* (**F**) and *me31B* (**G**) remained partialized stabilized. *$P < 0.05$, *n.s.* = not significant, n = 3, error bars = SD, Student's *t*-test.

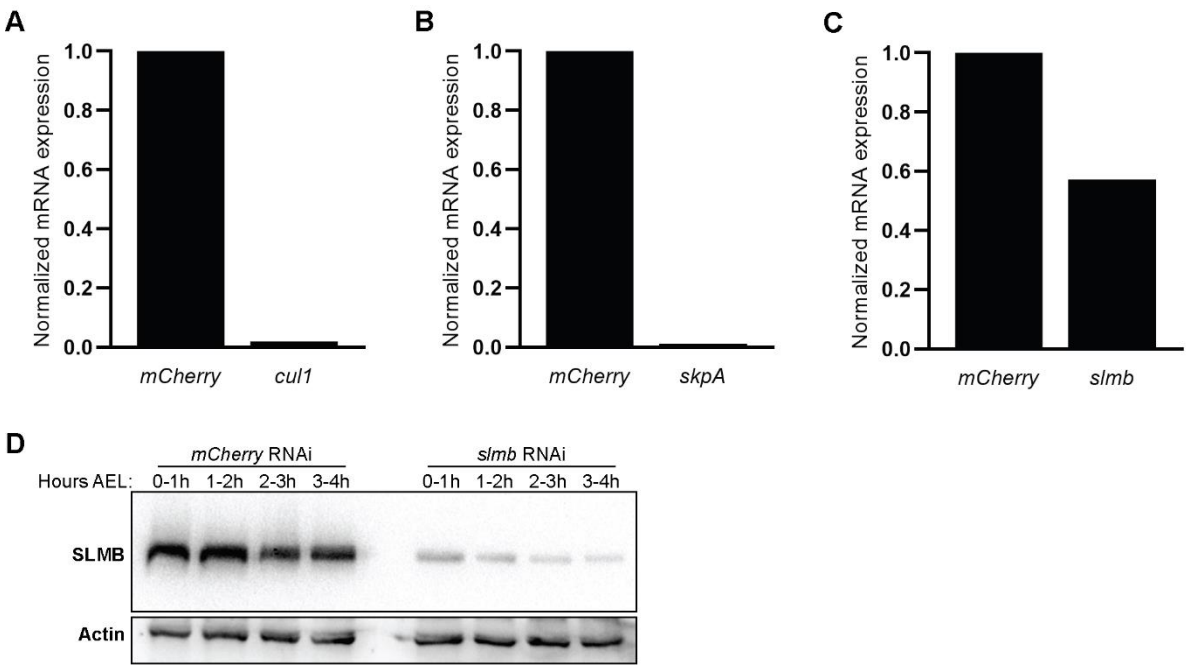

Figure S6. Validation of maternal RNAi knockdown of SCF complex members, related to Figure 5. RT-qPCR quantification of target mRNA expression in 0-3h embryos. **A.** *cul1* and **B.** *skpA* mRNAs were depleted by >98% relative to *mCherry* control RNAi in their respective maternal knockdowns. **C.** Maternal knockdown of *slmb* achieved a 43% reduction at the RNA level. **D.** Western blot of SLMB protein expression in *mCherry* control RNAi and *slmb* RNAi showed ~90% depletion of SLMB protein expression over the first 4 hours of embryogenesis resulting from the maternal *slmb* knockdown. Note: The same blot shown here is cropped and used in **Figure 6**.

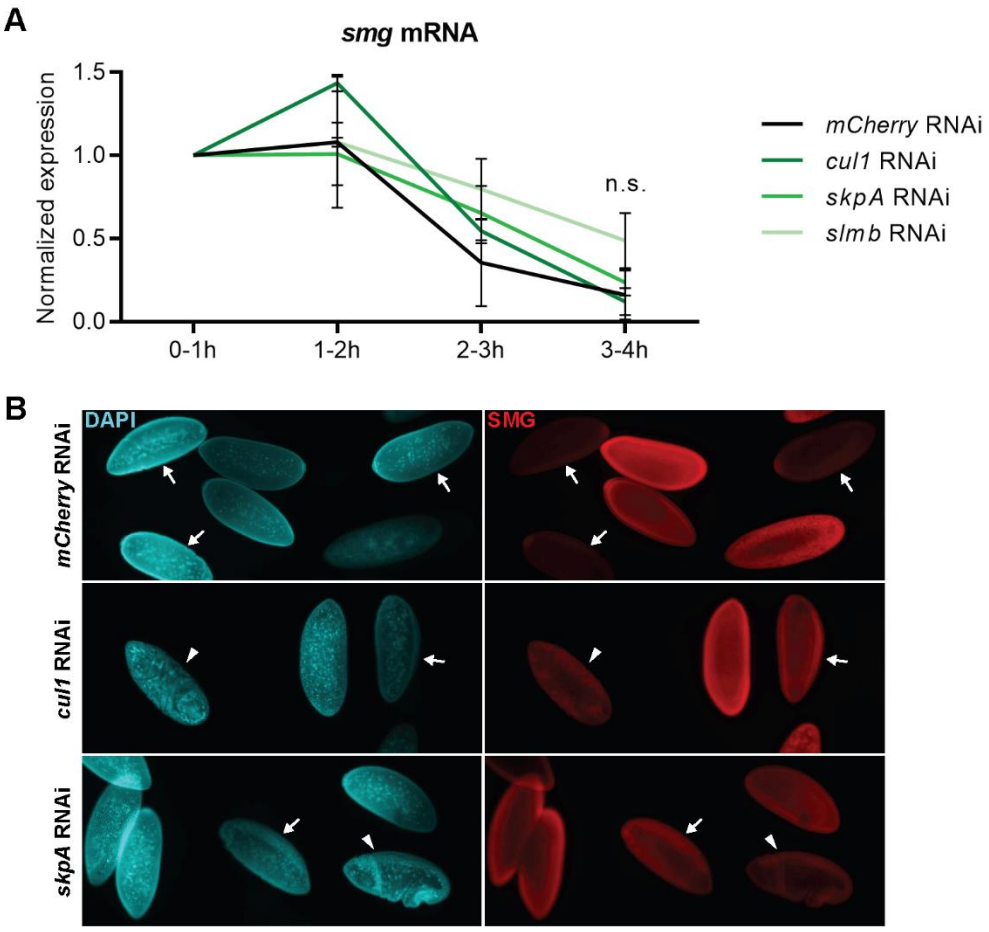

Figure S7. Knockdown of the SCF complex stabilizes SMG protein independent of RNA degradation and embryo development, related to Figure 5. A. RT-qPCR quantification of *smg* mRNA expression in embryos assayed in **Figure 5D**. Knockdown of the SCF complex had no significant effect on *smg* mRNA degradation relative to control knockdown. *n.s.* = not significant, n = 3, error bars = SD, Student's *t*-test. **B.** Immunofluorescence of nuclei (DAPI, blue) and SMG (red) in maternal knockdown embryos. In *mCherry* control knockdown, SMG was depleted from the blastoderm embryo by the onset of gastrulation (arrows). Knockdown of *cul1* or *skpA* resulted in ubiquitous persistence of SMG protein in comparable stages, as well as older gastrulating embryos (arrowheads).

Table S6, related to STAR Methods.

List of oligonucleotide primer sequences used for qPCR experiments.

Target gene	Forward primer	Reverse primer
RpL32	CTAAGCTGTCGCACAAATGGC	ACTTCTTGAATCCGGTGGGC
cup	TTCAAGCTGAAGGACGCACT	TTCAAGCTGAAGGACGCACT
tral	AAGTTCGAGGAACTGCGCTC	CCATTCAGTGTGTGAACGCC
me31B	GCCGAAAGCAAAAGAGAGCG	GATCATTTATAATCCCCTTGCTTGT
smg	GGTTGGATCTGCAGTTTTGC	TGGTTGCGTTGACGCTCTTA
muskelin	GCTGGAGGGTGGCCTAAAAA	TGCTGAAGTTGAACGACGGA
ranBPM	ATGAGCCGCAAGTTCGAGAT	CGGCTATAGCGTTTGCGTCT
CG3295	CAAGAAGTTTGCTGTGCGCT	ACGACAGTTCGGTCCACTTC
cul1	AGTCCACATGCGAAGAGGTT	ATCATCGTTTCGGTCTGCGT
skpA	AGTGCTCCGGCACTATCAAG	AATTCACATTGGGCAACGGC
slmb	AGCAAACGACGAGCCAGTAA	AGTGGTTGTGAAGGCCTGTG
Tom	ACTGGTCAAACCCCTTCTGC	ATCTTTGCGCATGTCCTCCA
CG12581	TGGCATCTACAAGCGCAAAG	CCACCATTTGGGCGATCTCA
Ama	TCCTATGTGGTTGGGTTGGC	CAATGCCTTGTCTCCTGGCT
CG5888	TTTGCCGACTCGGAGAACTG	AACGGGATATTCCTTGGCCTT
bru1	TGAACGCAAACTCTTTGTGG	GGCTCCGTGGACTTCAAATA
Mnt	CACAGGCCGACAAAGCAGTTT	GGCGTTGCCTGCATCGAAT
Hsp83	ACAACAAGCAGCGTCTGAAAAG	CCTGGAATGCAAAGGTCTCTG
CG4612	CACCAGTCACAAGCTCATGC	GACTGTGGGTTCTCGTAGGC
E(bx)	GTGCAACCGAACACCAGTAG	CTTCGGAATCCCCAAAATCT
Pcl	AAGCGAAGACTGAGTGCCAA	TGATGACCTCAATGGCCGTG
Grip84	AATCCGACACTACACCCGTA	GCTCAAGGATTGATCGGAAA
FBXO11	GACCCTCGCCAAAGATGTA	ACGAGAACGGACTTGGTCAG
Rpn2	ACCTCAAAAACACCGCTCCT	TATCATCAGCTGGCGTCTCC
Rpn7	GACCAAAATGCCTGCCGAAA	ATGCCGCATCCTGCTTGTAT
CBP	CCATCGTGAGCCGTGGTATT	GATGCCAGGCGGTGACAATC
Pex11	CAGCGCTTGTGGACAACTT	TCTTCAGAGCGCCGTAGAAT
morgue	GGACCAGGAACACCACCA	AAGTTGGGCCCATAGTAGCC
cpa	ACTCTGCTAAAGGATGGGGC	TAGAAGCGACCGTTTCCCAG
CG13472	GGGCCTTAAAATCGTGACAA	AATATTTCGCACACGCTGAA
oys	GCAAAATGCTAGAACCGCCG	AGTTTACCAAGTCCACGGAGAG
Hmt4-20	TGGAAAGAGACGGACACACG	ACCATTCTGCACGACAGTCTTA